MECHANICAL BEHAVIOR OF ADHESIVE JOINTS SUBJECTED TO THERMAL CYCLING

G. Robert Humfeld, Jr.

Thesis submitted to the Faculty of the Virginia Polytechnic Institute and State University in partial fulfillment of the requirements for the degree of

Master of Science
in
Engineering Mechanics

D. A. Dillard, Chairman
V. Giurgiutiu
T. C. Ward

February 7, 1997
Blacksburg, Virginia

Keywords:
thermal cycling, adhesive bond, polymer, residual thermal stress, viscoelasticity, fracture mechanics, thermal ratchetting

Copyright 1997, G. Robert Humfeld, Jr.

MECHANICAL BEHAVIOR OF ADHESIVE JOINTS SUBJECTED TO THERMAL CYCLING

G. Robert Humfeld, Jr.

(ABSTRACT)

The effect of thermal cycling on the state of stress in polymeric materials bonded to stiff elastic substrates was investigated using numerical techniques, including finite element methods. The work explored the relationship between a cyclic temperature environment, temperature-dependent viscoelastic behavior of polymers, and thermal stresses induced in a constrained system. Due to the complexity of developing a closed-form solution for a system with time, temperature, material properties, and boundary conditions all coupled, numerical techniques were used to acquire approximate solutions. Descriptions of attempted experimental verification are also included.

The results of the numerical work indicate that residual stresses in an elastic-viscoelastic bimaterial system incrementally shift over time when subjected to thermal cycling. Tensile axial and peel stresses develop over a long period of time as a result of viscoelastic response to thermal stresses induced in the polymeric layer. The applied strain energy release rate at the crack tip of layered specimens is shown to similarly increase. The rate of change of the stress state is dependent upon the thermal cycling profile and the adhesive's thermo-mechanical response. Discussion of the results focuses on the probability that the incrementing tensile residual stresses induced in an adhesive bond subjected by thermal cycling may lead to damage and debonding, thus reducing durability.

This work has been supported by the Adhesion and Sealant Council, the Center for Adhesion and Sealant Science, and the National Science Foundation: Science and Technology Center (contract DMR 9120004).

ACKNOWLEDGMENTS

I would like to thank Dr. David Dillard for his guidance and encouragement. His commitment to excellence in research is a challenging standard to which I aspire. Help and advice from Dr. Tom Ward, Dr. Garth Wilkes, Dr. John Dillard, and Dr. Victor Giurgiutiu are also gratefully acknowledged.

I would like to acknowledge the financial support of the Adhesion and Sealant Council, the Center for Adhesion and Sealant Science, and the National Science Foundation: Science and Technology Center (contract DMR 9120004).

Well-deserved thanks go to Mr. Raúl Andruet, Mr. Tsunou Chang, and the other past and present members of the Adhesion Lab who have taught me essential skills, contributed useful comments, or simply leant moral support.

Finally, a special thanks goes to Mr. Charles Randow to whom I have looked often for inspiration, encouragement, and advice.

Table of Contents

ACKNOWLEDGMENTS III

TABLE OF CONTENTS IV

LIST OF FIGURES VI

CHAPTER 1 - INTRODUCTION 1

CHAPTER 2 - PROBLEM DEFINITION 3

CHAPTER 3 - THERMOVISCOELASTIC ANALYSIS OF A 1-D BAR 6

3.1 GEOMETRY 6
3.2 DERIVATION OF THE RECURSIVE EQUATION 6
3.3 EXAMPLE RESULTS 9
3.4 STEADY-STATE ANALYSIS 12
3.5 PARAMETER SENSITIVITY 15
3.6 THERMAL PROFILE SENSITIVITY 19

CHAPTER 4 - FINITE ELEMENT SOLUTION 22

4.1 THE MESH 22
4.2 ABAQUS RESULTS 23

CHAPTER 5 - COMPARISON OF 1-D AND 2-D ANALYSIS RESULTS 26

CHAPTER 6 - FRACTURE ANALYSIS 27

CHAPTER 7 - DISCUSSION OF ANALYSIS RESULTS 35

CHAPTER 8 - EXPERIMENTAL VERIFICATION 37

8.1 STRATEGY 37
8.2 PROCEDURES 38
8.3 PROBLEMS AND SOLUTIONS 39
8.3.1 Problems With Mixing 39
8.3.2 Problems With Cure Time 39
8.3.3 Problems With Consistency 40
8.4 EXPERIMENTAL RESULTS 40

CHAPTER 9 - CONCLUSION 43

CHAPTER 10 - RECOMMENDATIONS FOR FUTURE WORK 44

REFERENCES 45

APPENDIX A: MATHEMATICA ROUTINE 48

APPENDIX B: ABAQUS INPUT FILE - STRESS BUILD-UP 51

APPENDIX C: ABAQUS INPUT FILE - SERR STUDY 56

APPENDIX D: EXPERIMENTAL RESULTS...65

VITA...75

LIST OF FIGURES

FIGURE 1. CONTRACTION OF THE ADHESIVE LAYER AFTER DEBONDING DUE TO THERMAL CYCLING 1
FIGURE 2. AXIALLY-CONSTRAINED VISCOELASTIC BAR 6
FIGURE 3. MAXWELL ELEMENT 7
FIGURE 4. CTE VS. TEMPERATURE (POLYMER) 9
FIGURE 5. TEMPERATURE PROFILE - ONE CYCLE OF THE NEAR-SQUARE "TANH-WAVE" 10
FIGURE 6. STRESS DEVELOPMENT OVER 3 CYCLES 11
FIGURE 7. STRESS DEVELOPMENT OVER 50 CYCLES 11
FIGURE 8. STRESS VS. TIME DURING STEADY STATE CYCLE 13
FIGURE 9. T_G SENSITIVITY CURVE FOR CYCLING BETWEEN T_C AND T_H 16
FIGURE 10. T_G SENSITIVITY CURVE WITH CYCLING TIME (CYCLING BETWEEN T_C AND T_H) 16
FIGURE 11. STRESS VS. TIME FOR T_G=27°C 17
FIGURE 12. STRESS VS. TIME FOR T_G=57°C 17
FIGURE 13. STRESS VS. TIME FOR T_G=87°C 18
FIGURE 14. STRESS VS. TIME FOR T_G=117°C 18
FIGURE 15. STRESS DEVELOPMENT - TANH WAVE 19
FIGURE 16. STRESS DEVELOPMENT - SINE WAVE 20
FIGURE 17. T_G SENSITIVITY CURVE FOR DIFFERENT THERMAL PROFILES 21
FIGURE 18. 2-D FINITE ELEMENT MESH OF ONE QUARTER OF A SANDWICH GEOMETRY 22
FIGURE 19. AXIAL STRESS DISTRIBUTION AFTER TEN CYCLES 23
FIGURE 20. PEEL STRESS DISTRIBUTION AFTER TEN CYCLES (FREE END OF SPECIMEN) 24
FIGURE 21. SHEAR STRESS DISTRIBUTION AFTER TEN CYCLES (FREE END OF SPECIMEN) 24
FIGURE 22. PEEL STRESS DISTRIBUTION (COLD TEMP.) FOR INCREASING NUMBERS OF THERMAL CYCLES 25
FIGURE 23. SHEAR STRESS DISTRIBUTION (COLD TEMP.) FOR INCREASING NUMBERS OF THERMAL CYCLES 25
FIGURE 24. HALF OF SANDWICH WITH PRE-CRACKS AT END 27
FIGURE 25. SANDWICH GEOMETRY CROSS-SECTION 28
FIGURE 26. SANDWICH GEOMETRIES WITH EQUAL STORED STRAIN ENERGIES 30
FIGURE 27. STRAIN ENERGY RELEASE RATE FOR LAYERED SPECIMENS AFTER THERMAL CYCLING 33
FIGURE 28. DETAILS AFFECTING RATE OF STRESS DEVELOPMENT 36
FIGURE 29. DETAILS AFFECTING MAXIMUM MAGNITUDE OF BUILT-IN STRESSES 36
FIGURE 30. TYPICAL DCB FRACTURE SURFACE FROM TESTING AT ROOM TEMPERATURE 41
FIGURE 31. INTERESTING DEBONDING PATTERNS FOR SPECIMENS TESTED AT -40°C 42
FIGURE 32. DMA DATA, FIRST HEATING CYCLES 66
FIGURE 33. DMA DATA, SECOND HEATING CYCLES 67
FIGURE 34. DSC DATA, FIRST AND SECOND HEATING CYCLES 68
FIGURE 35. DDSC DATA, FIRST HEATING CYCLE 69
FIGURE 36. DDSC DATA, SECOND HEATING CYCLE 70
FIGURE 37. PLOT OF TYPICAL QUASI-STATIC DCB LOADING CURVE 71
FIGURE 38. DATA FIT FOR TYPICAL COMPLIANCE METHOD DCB ANALYSIS 72
FIGURE 39. DATA ACQUIRED FROM QUASI-STATIC DCB TESTING OF AL-PUR BONDS 73
FIGURE 40. PLOT OF G VS. TIME FOR SUB-AMBIENT DCB TEST 74

Chapter 1 - Introduction

Thermal changes affect adhesive bonds in two ways: by inducing thermal stresses in the system and by changing the mechanical properties of the viscoelastic adhesive. This paper investigates the interaction between these effects and identifies the possibility of the evolution of residual stresses toward a more tensile stress state as a result of thermal exposure. These alterations in the residual stress state have the potential to contribute to reduced life of adhesive bonds and polymeric materials in a variety of applications.

The study was prompted by reports from industry contacts that cyclic thermal testing was leading to spontaneous failure of adhesive sandwich specimens. The specimens were observed to remain sound for an initial period of thermal cycling, until debonds developed along each interface at the free edges. The length of the debonds steadily grew as testing continued. Once it had completely debonded from its substrates, the adhesive layer was observed to be noticeably shorter than its original length (Figure 1). Neat polymer specimens subjected to identical thermal loading were reported to have undergone no similar dimensional changes.

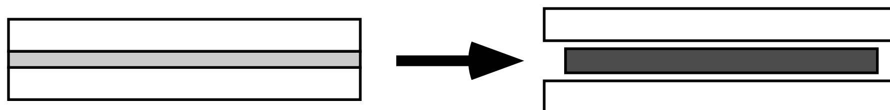

Figure 1. Contraction of the adhesive layer after debonding due to thermal cycling.

The author hypothesizes that the observed behavior in the bonded system is due to the fluctuating mechanical behavior of the polymer during thermal cycling. Debonding is believed to be caused by thermal stresses resulting from a mismatch of the coefficients of thermal expansion (CTE) of the adhesive and substrate(s). These stresses will be shown to increase in severity over a number of cycles. Contraction of the adhesive layer after or during debonding is postulated to be evidence of viscoelastic flow occurring in the adhesive during thermal cycling. Were other changes in the adhesive (i.e. volume loss, aging, decomposition, etc.) responsible, contraction should also have been evident in the neat specimen.

Thermal and residual stresses have been the subject of much study in the last 70 years. Thermal stresses in bimetal systems have been widely examined, first by Timoshenko [1] in 1925. Analyses of increasing complexity followed, considering systems with interfacial cracking [2], more complicated geometries [3], and transverse stress considerations [4,5]. These works all found that heating a bimetal strip induces axial stresses in the system components - tensile in one and compressive in the other. These stresses run parallel to the interface with nearly constant magnitudes along most of the center length and a drop off to zero near the edges. Shear stress

was found to be zero along the interface except near the edges, where it reaches maximum values. Analysis of transverse stresses by Suhir predicted high tensile peel stresses at the free edges, with a small compressive region between the end and the constant stress center region, where peel is zero. All of these analyses applied to systems containing no components with time- or temperature-dependent material properties.

Investigation of temperature- and time-dependent behavior of polymeric material systems subjected to thermal changes is widely available. A good analytical overview can be found in a paper by Losi and Knauss [6]. Struik's experimental study of "frozen-in" deformations in polymers [7] is the most directly relevant to this study. He applied a constant creep stress to polymer specimens while subjecting them to changing temperature. Creep compliance and recovery predictions by analysis similar to that used in this paper were found to match experimental results reasonably well. The reader may also be interested in works relating to cooling and curing stresses [8,9,10], some of which include consideration of thermal conduction, a factor neglected in this paper for simplicity.

Thermal cycling as a source of damage in material systems has been reported for a wide variety of situations. Failure in plastic packaging [11], solder joints [12], and thermal barrier films [13] has been attributed to thermal cycling, but without specific mechanisms of failure being identified. Thermal fatigue [14] and thermal ratchetting [15] are two failure mechanisms that have been identified in materials subjected to the thermal cycling - the former describing incremental crack growth in constrained materials and the latter defining plastic strain accumulation in metals cycled at very high temperatures. An analytical study of the effect of thermal cycling on elastic bimaterial systems has been presented by Ryan and Mall [16].

Thermal cycling effects and non-linear material response are considered together in some works. A paper by Suresh [17] contains closed-form and finite element elasto-plastic analyses of layered materials subjected to thermal cycling. Inelastic strain accumulation in short fiber metal matrix composites during thermal cycling has been considered by Dunn and Taya [18]. A study of the thermo-viscoelastic response of graphite/epoxy composites during thermal cycling has been authored by Lin and Huang [19]. However, a definitive treatment of the problem of a viscoelastic-elastic bimaterial system subjected to thermal cycling does not appear to exist in the current body of literature.

This work is an attempt to add to the current understanding of thermal and residual stress development in polymeric coatings and adhesive bonds by considering the effects of temperature-dependence and viscoelastic flow during thermal cycling. An understanding of the development of stress over time at an elastic-viscoelastic bimaterial interface subjected to a cyclic thermal profile could contribute to more effective design and failure analysis for a wide variety of applications and is therefore of compelling interest and importance for the adhesives industry.

Chapter 2 - Problem Definition

The problem considered is that of a polymeric layer bonded to one substrate as a coating or between two substrates as an adhesive. The substrate material is assumed to be elastic and relatively stiff (e.g. a metal). The polymeric adhesive or coating is assumed to be a thermorheologically simple, linear viscoelastic, isotropic material. The entire system is subjected to a cyclic temperature profile (e.g. square-wave, sine-wave) and expands and contracts with the changes in temperature. Stresses are induced at each interface as a result of CTE mismatch and in-plane strain, shear stress, and peel stress matching conditions required at the bond interfaces.

Determining the complete state of stress over time for such a problem is no trivial task; including a viscoelastic component introduces complexities beyond the classic stress distribution problem. One must also consider temperature-dependence of material properties and viscoelastic flow over time. A complete stress solution must therefore include five independent variables: position (x,y,z), temperature, and time. Solving the stress distribution problem normally requires knowing the geometry of the bond and the CTE and stiffness of the adhesive and substrate(s). But it also requires determining the instantaneous temperature and instantaneous stiffness of the adhesive for the point in time of interest, and requires including the effects of the entire thermo-viscoelastic loading history to that point.

Stress magnitudes will vary through the thickness, across the width, and along the length of the bond. The shape of the stress distributions will be determined by the boundary conditions and the conditions of axial strain, peel stress, and shear stress continuity across the bond interface. Considering the distributions along the length from a free end toward the center of an adhesive layer, stress gradients will be concentrated near the free end. Axial stress will be zero at the free ends but quickly rise to a maximum value away from the end, remaining constant across most of the length. Shear stress will be zero at the end, first steeply rising to its maximum value and then quickly falling away again to zero as the axial stress levels off to its maximum. Peel stress will be at its maximum at the free end, fall steeply into a small region of opposite magnitude, and then decay to zero away from the end. The reader seeking further detail of thermally induced stress distributions in bimaterial systems is referred to the work of Suhir [4,5]

For uniaxial loading, the stress as a function of time in a linear viscoelastic material given a varying applied strain may be expressed with a hereditary integral:

$$(x,t) = {}^{t}_{-} E(t - \ ) — [\ (x, \ ) - \tilde{\ }(x, \ )] \ d \qquad [1]$$

where the variables are defined:

E stiffness tensor
e total applied strain
$\tilde{}$ thermal strain.

The hereditary integral can be used to express stress at any time given any arbitrary loading history. The difficulty in applying equation 1 to our problem lies in including the loading history through a correct expression of applied strain. The applied strain along the boundary of the adhesive interface is difficult to derive.

Temperature will determine both the stress level and the rate of viscoelastic response of the adhesive to that stress level. The temperature-dependence of a polymer's mechanical behavior is commonly accounted for by applying the Time-Temperature Superposition (TTSP) principle. The constitutive equation (1) is modified by scaling the time variable by a "shift factor" (commonly denoted a_T) which is defined as the ratio of reduced time to real time for a material as a function of temperature. It can be taken directly from experimental data or modeled using any one of many analytical methods. Adding the shift factor to the constitutive equation yields:

$$(x,t) = \int_{-}^{t} E(\ (x,t) - \ (x,\ ))\ -[\ (x,\ ) - \tilde{}(x,\ )]\ d \qquad [2]$$

where

$$(x,t) = \int_{-}^{t} a_T(T(x,\ ))\ d \qquad \text{and} \qquad (x,\ ) = \int_{-} a_T(T(x,\ ))\ d$$

and the variables are defined:

T temperature
a_T shift factor

Equation 2 is still an exact expression. In order to evaluate it for an adhesive bond subjected to thermal cycling, proper equations describing thermal conduction and continuity of in-plane strains and shear and peel stresses across a bimaterial interface would still need to be included before integration. As can be imagined, analytically evaluating the combination of such expressions is complex to the point of being practically impossible.

Before any solution was attempted, some basic assumptions were made to simplify the problem. Thermal conduction was assumed to be an instantaneous process, resulting in spatially uniform temperatures (and therefore thermal strains) throughout. The coefficient of thermal expansion was assumed to be independent of time. The geometries were assumed to be stress-

free before any thermal cycling was applied. Other assumptions were made in each of the solution approaches and are explained in the appropriate chapters.

Of the assumptions, the instantaneous thermal conduction assumption is the most serious. In reality, heat sources and sinks would exist outside of an adhesive bond and conduction would take place through the bond. In most cases, a metallic substrate would have a greater conductivity than a polymeric adhesive. This may lead to greater thermal strain mismatches in the materials near the bond interface(s) than are predicted by assuming instantaneous conduction. It is recommended for future work in this area that the effect of the inclusion of finite thermal conduction be explored.

Two methods were used in this paper to obtain solutions for such problems: simplification of the problem geometry to eliminate position-dependence and finite element analysis to obtain solutions for the more complex geometry. In both cases, numerical methods were used so the results are approximate rather than exact solutions.

Chapter 3 - Thermoviscoelastic Analysis of a 1-D Bar

3.1 Geometry

One approach was to simplify the problem by considering the polymeric layer as a viscoelastic bar with constraints preventing any thermal expansion or contraction in the axial direction (Figure 2).

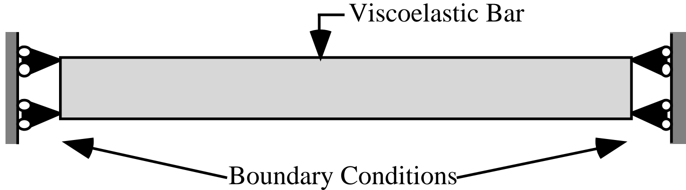

Figure 2. Axially-constrained viscoelastic bar

This simplified problem has constraints similar to those in the center of a real bond and is worthwhile because it focuses on the influence of viscoelastic relaxation on the stresses induced by thermal cycling independent of geometry dependencies. Analysis is simpler because stress is one-dimensional, uniform along the length of the bar, and induced by constraints acting independent of time and temperature. The results can give insights into problems with more complicated boundary conditions.

3.2 Derivation of the Recursive Equation

Total strain in a system is the sum of two components: mechanical strain ($_M$) and thermal strain ($_T$).

$$= {}_M + {}_T \qquad [3]$$

Given the bar has fixed ends, the total axial strain ( ) is always zero. Mechanical strain must therefore always be equal and opposite to the thermal strain:

$${}_M = - {}_T = - {}^{T}_{T_0} (T)\, dT \qquad [4]$$

where T_0 initial temperature (initially stress- and strain- free).

The Maxwell element was selected as the mechanical model for this material because the problem most nearly resembles a stress relaxation problem.

Figure 3. Maxwell Element

The derivation of the recursive relationship builds of the work of Zeinkiewicz for a Kelvin element [21]. The governing differential equation for a Maxwell element is:

$$\dot{\sigma} + \frac{E}{\eta}\sigma = E\dot{\varepsilon} \qquad [5]$$

where $\dot{\varepsilon}$ is defined:

$$\dot{\varepsilon} = \frac{\Delta\varepsilon_M}{\Delta t} = -\frac{\Delta\varepsilon_T}{\Delta t} \qquad [6]$$

Let σ_i be the stress at $t = t_i$, we can determine the stress σ_{i+1} at $t = t_i + \Delta t$ by integrating:

$$\int_{\sigma_i}^{\sigma_{i+1}} d\sigma = \int_{t_i}^{t_i+\Delta t} \left[E\dot{\varepsilon} - \frac{E}{\eta}\sigma(t)\right] dt \qquad [7]$$

If we assume that $\dot{\varepsilon}$ is constant over the time step Δt, integration yields the equation

$$\sigma_{i+1} - \sigma_i = E\dot{\varepsilon}\Delta t - \frac{E}{\eta}\int_{t_i}^{t_i+\Delta t} \sigma(t)\,dt \,. \qquad [8]$$

The assumption that $\dot{\varepsilon}$ is constant over Δt will control how small Δt must be for a given temperature profile to obtain a reasonably accurate solution.

Stress as a function of time can be determined from the governing differential equation (again assuming that $\dot{\varepsilon}$ is constant):

$$\sigma(t) = Ae^{\frac{-t}{\tau}} + \eta\dot{\varepsilon} \qquad [9]$$

where $\tau = \frac{\eta}{E}$ is the characteristic relaxation time of the Maxwell element and A is a constant determined by the initial condition $\sigma(t_i) = \sigma_i$:

$$A = \frac{_{i} - \;\dot{}}{e^{\frac{-t_i}{}}} \qquad [10]$$

Completing the integration of (t) and manipulating the resulting equation yields the recursive relation:

$$_{i+1} = \; _{i}e^{\frac{-t}{}} + \; \dot{}_{i}\left(1 - e^{\frac{-t}{}}\right) \qquad [11]$$

In order to account for temperature-dependence, the time variables are scaled by a_T, giving the final form of the equation:

$$_{i+1} = \; _{i}e^{\frac{-t}{a_T}} + a_T \; \dot{}_{i} \; 1 - e^{\frac{-t}{a_T}} \qquad [12]$$

where

$$\dot{}_{i} = -\frac{d_{T}}{dt}\bigg|_{t=t_i} = - \; \left(T(t_i)\right)\frac{dT(t)}{dt}\bigg|_{t=t_i} \qquad [13]$$

This equation can be used to track the development of stress by using a time-stepping process. It can be used with any temperature profile, but is only valid for the axially-constrained geometry. The stability and accuracy of the solution are determined by the size of the time step. If the time step is selected to be small enough to insure the that $\dot{}$ is nearly constant for every increment t, then stable and reasonably accurate solutions are obtained.

This derivation can easily be extended to a generalized Maxwell element. Total stress in a generalized Maxwell element is the sum of the stresses in all components. Each component is subjected to the same strain profile, so each is independently governed by the recursive equation derived above. The equation for a generalized Maxwell element is therefore a summation of recursive equations of all of its elements:

$$_{i+1} = \sum_{j=1}^{n} {}^{(j)}_{i+1} = \sum_{j=1}^{n} {}^{(j)}_{i}e^{\frac{-t}{a_T \; ^{(j)}}} + a_T \; ^{(j)}\dot{}_{i} \; 1 - e^{\frac{-t}{a_T \; ^{(j)}}} \qquad [14]$$

where j represents the element number, n is the total number of elements, and $\dot{}_{i}$ is defined in equation 13.

3.3 Example Results

The recursive equation was used to predict stress development in a constrained polyurethane bar. Different polyurethanes have a wide variety of mechanical properties. For this study, mechanical properties were selected to roughly model material data provided us by industry experts who had observed debonding and contraction in sample specimens. Realistically, a single Maxwell element was a very poor model for the polyurethane, but an exact match was not considered essential as the purpose of the study was not a perfect prediction of stress in a real material, but a basic understanding of how a model material might react to the thermal cycling. Material properties selected were:

$E = 1$ MPa
$= 1$ sec at T_g
$T_g = 87°C$

CTE was assumed to be $100x10^{-6}$ $°C^{-1}$ in the glassy region and 200 $x10^{-6}$ $°C^{-1}$ in the rubbery region, with the exact curve defined by the equation:

$$(T) = 50x10^{-6}\left(3 + \mathrm{Tanh}\left[\tfrac{3}{5}\left(T - T_g\right)\right]\right) \qquad [15]$$

which has the shape:

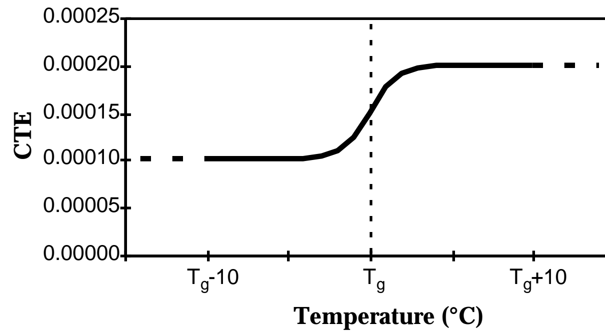

Figure 4. CTE vs. Temperature (polymer)

The Williams-Landel-Ferry (WLF)[22] equation was used to model the temperature shift factor,

$$\mathrm{Log}\ a_T = \frac{C_1(T - T_g)}{C_2 + T - T_g} \qquad [16]$$

and the C_1=20 and C_2=100°C were used in the analysis. It is not exactly correct to use the WLF equation for temperatures below the glass transition, but it was again only used because it is convenient for illustration purposes.

The temperature profile applied was that of a symmetric, near-square wave cycling between T_o=27°C and T_1=70°C with a period of one hour, each cycle defined by the equation:

$$T(t) = 27 + 21.5\ \mathrm{Tanh}\ \frac{t-900}{120}\ - \mathrm{Tanh}\ \frac{t-2700}{120} \qquad [17]$$

which is plotted below:

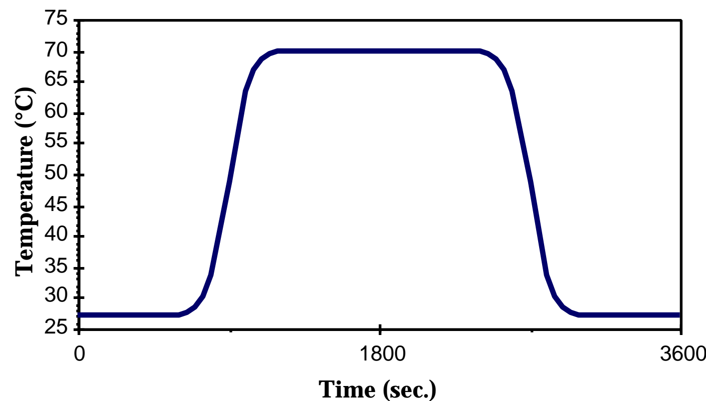

Figure 5. Temperature Profile - one cycle of the near-square "Tanh-wave"

It will be noticed that equation 17 is not a cyclic function; each cycle of the function was defined so that for any integer n,

$$T(n\,3600 \quad t \quad (n+1)\,3600) = T(0 \quad t \quad 3600)$$

The Mathematica program developed to solve the problem is included as Appendix A. The time step used in the program (t in equation 12) was 20 seconds. Convergence was confirmed by comparing to solutions using time step of 1 second. Over the course of three cycles, there was less than one percent difference between the solutions.

The results of the recursive solution method are presented below; stress in the axially-constrained polymer is plotted against time for three thermal cycles (Figure 6) and 50 thermal cycles (Figure 7).

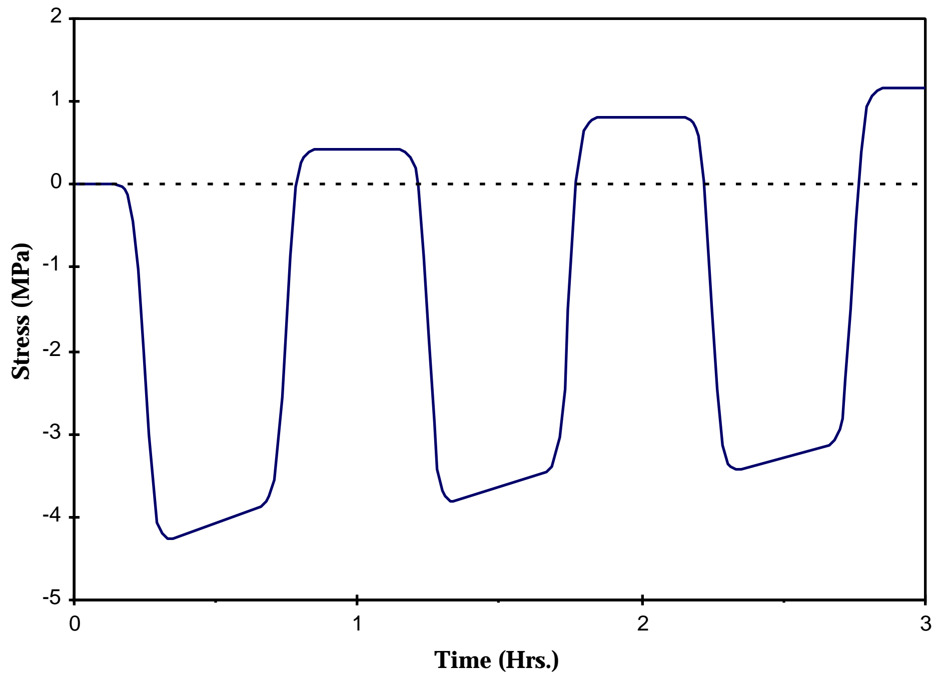

Figure 6. Stress development over 3 cycles

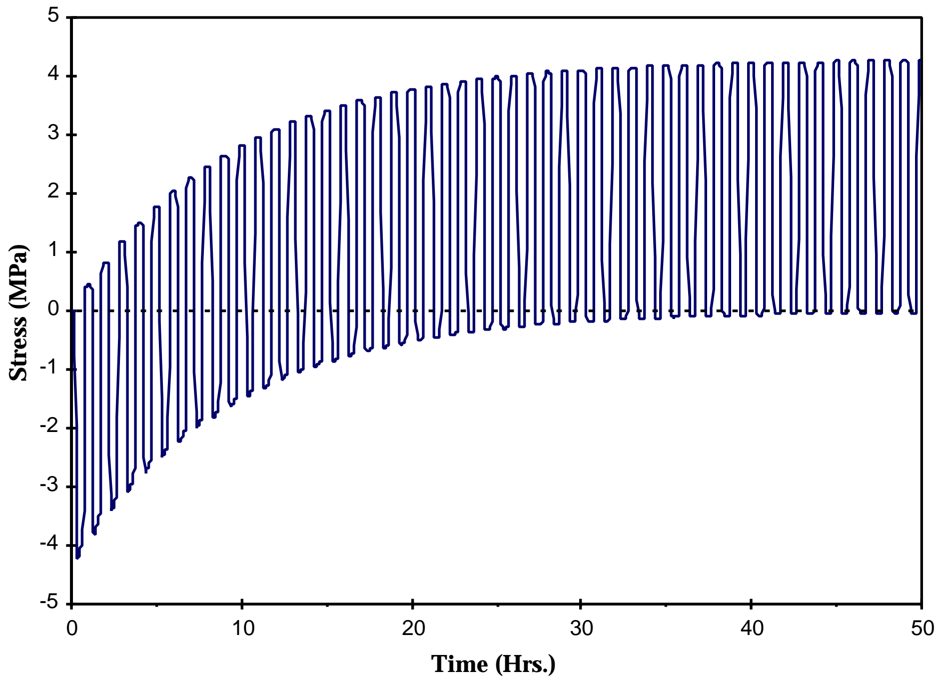

Figure 7. Stress development over 50 cycles

Increasing the temperature induces a compressive axial stress in the bar because thermal expansion is prevented by the end constraints. These compressive stresses relax at an accelerated rate due to the increased temperature. When the material is cooled, stress relaxation at the hot temperature is reflected in increased residual tensile stresses at the cold temperature. These stresses cannot be fully relieved before the next cycle begins because of the slow rate of relaxation at colder temperatures. Each full temperature cycle therefore results in an increased tensile residual stresses at the low temperature, a condition which may eventually cause or contribute to bond failure.

The reader is reminded that the exact magnitudes of stress in this example problem are not important; the trends are important. Different systems would have different material properties which would result in different stress levels. However, regardless of the stress magnitudes or amount of time cycled, the trend of tensile stress development in viscoelastic adhesives during thermal loading is one that should basically be universal. More detailed examination of this phenomenon follows.

3.4 Steady-State Analysis

The tensile residual stress in the polymer layer at the cold temperature asymptotically levels off over time. The value of the asymptote represents the maximum stress level that could exist in the specimen as a result of the given thermal profile. This is the same stress that would occur in the material if it reached steady-state thermoviscoelastic oscillation. Whether stress ever reaches the steady-state asymptote value depends upon the properties of the polymer, the thermal history, and the time in the cycling environment. Although it may never be truly realized, the steady-state cycle is useful to consider because it corresponds to the worst-case scenario for tensile stress development for a given problem.

For the simplified geometry described above, the generalized thermoviscoelastic equation reduces to the integral equation:

$$(t) = - {}_0^t E(\ \ -\ \ )\ \ (T(\ \ ))\ \frac{T(\ \ )}{}\ d \qquad [18]$$

For a material system at steady-state,

$$(t + nP) = \ \ (t) \qquad [19]$$

where P is the period of the thermal cycle and n can be any positive integer.

For n=1,

$$(t+P) \;=\; (t) \;-\; {}_{t}^{t+P}E(\; - \;) \;\; (T(\;)) \; \frac{T(\;)}{} \, d \qquad [20]$$

or,

$${}_{t}^{t+P}E(\; - \;) \;\; (T(\;)) \; \frac{T(\;)}{} \, d \; = 0 \qquad [21]$$

During steady-state cycling, the cumulative change in stress over any number of complete thermal cycles will always be zero. Determining the stress magnitudes using this relationship for arbitrary materials and thermal profiles is not straightforward. The case of a single Maxwell element subjected to a square-wave thermal profile is easily solved , however, and is presented below.

For a square wave thermal profile, there are instantaneous jumps in strain (since the CTE is not time-dependent) and shift factor, thus simplifying the hereditary integral:

$${}_{h_o}(1 - e^{\frac{-P}{2a_{T_h}}}) + {}_{c_o}(1 - e^{\frac{-P}{2a_{T_c}}}) = 0 \qquad [22]$$

where the new variables are defined:

$_{h_o}$	instantaneous initial value of stress at the hot temperature
$_{c_o}$	instantaneous initial value of stress at the cold temperature
a_{T_h}	shift factor at the hot temperature
a_{T_c}	shift factor at the cold temperature

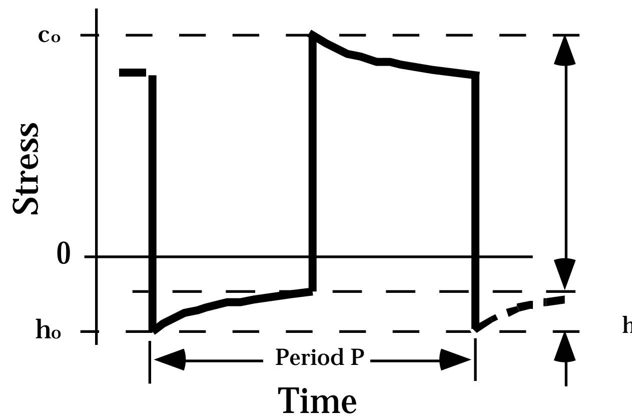

Figure 8. Stress vs. Time during steady state cycle

The difference in the initial stress magnitudes is

$$ {}_{c_o} - {}_{h_o} = {}_{T} + {}_{h} \qquad [23]$$

where the new variables are defined:

$_T$ change in thermal strain for one ramp
$_h$ change in stress at hot temperature due to relaxation

The total change in stress magnitude for one stress ramp will depend upon the thermal profile. $_T$ is normally time-dependent and evaluated using equation 18. For a square-wave thermal profile in which temperature rises nearly instantaneously, thermal stress can be expressed merely as a function of temperature. If thermal loading is truly instantaneous, the modulus of the adhesive will allow for no relaxation; thermal stress would be a product of thermal strain and the glassy modulus. The author wanted to take a temperature-dependent modulus into account to compare to the recursive solution results, so the one-second modulus was used in the integral to determine change in thermal stress during one temperature ramp. Solving equation 23 for the cold-temperature stress yields:

$$ {}_{c_o} = \frac{{}^{T_h}_{T_c} E_{1sec}(T)\quad (T)\, dT}{2 - e^{\frac{-P}{2a_{T_c}}} - \dfrac{1 - e^{\frac{-P}{2a_{T_c}}}}{1 - e^{\frac{-P}{2a_{T_h}}}}} \qquad [24]$$

Applying equation 24 to the previously described example problem yields a predicted maximum stress of 4.30 MPa. This is very close to the maximum value of 4.27 MPa returned by the recursive equation (predicted by evaluating until very near steady-state conditions). One would expect equation 24 to overpredict the maximum stress, as nearly instantaneous changes in temperature (i.e. ramping in one second) during a thermal profile are uncommon. For slower thermal ramping, stresses will begin to relax even as they are increasing during cooling from hot to cold temperature, resulting in a decreased maximum amplitude than would result from quicker cool-down. Further discussion of the rate of thermal ramping and the applicability of equation 24 is contained in the section 3.6.

3.5 Parameter Sensitivity

One way in which an understanding of residual stress predictions could be used is for material selection criteria for any given application. Materials could be selected or developed based on criteria such as stiffness, CTE, and T_g that would minimize the residual stress magnitudes or delay the rate of viscoelastic relaxation (increasing the time to maximum stress). It is therefore useful to investigate the effects of changing these parameters independent of one another.

The effect of varying the CTE is evident; increased CTE results in increased strain and therefore increased stress while decreasing CTE has the opposite effect. The CTE of polymers change at the glass transition point, often doubling or quadrupling, significantly increasing the thermal strain mismatch with the substrate material. However, despite the increased rubbery CTE, the magnitude of the glassy CTE is the more important parameter. This is because while CTE increases, relaxation rate is radically increasing, and the stress induced relaxes out very quickly.

Let us consider a problem where the bond geometry can be modeled by the recursive solution derived in the previous section. Let us also allow that the thermal profile for the application is known, say the thermal profile used in the previous section. If we could select between materials which had exactly the same material properties except for the glass transition temperature, how would the development of residual stresses vary between the specimens?

For Tg below the low temperature cycling limit, all changes in thermal stress and strains occur while the adhesive is rubbery and viscoelastic flow is nearly instantaneous. No significant buildup of residual stresses would occur in this region for a viscoelastic fluid. At the other extreme, when the material is glassy for the entire thermal ramp, the maximum stress possibly built into the system without mechanical loading will be the simple product of glassy stiffness, CTE, and temperature difference. For the case currently being considered, that product yields a stress of 4.3 MPa.

In order to examine the dependence of maximum stress on Tg, a series of numerical analyses were run for the example problem of section 3.3. The only parameter that was varied was Tg. Results of the analyses at multiple glass transition temperatures are plotted in Figure 9, along with the analytical curve from equation 24. The dashed lines represent the values between which temperature is being cycled.

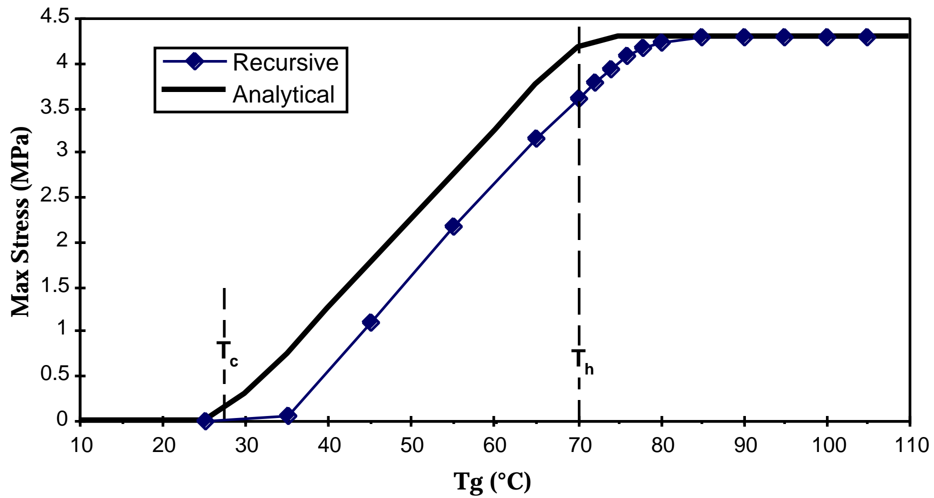

Figure 9. T_g Sensitivity Curve for Cycling between T_c and T_h

The data follow the trend expected, with an insignificant stress level when Tg is very low and a maximum (4.30 MPa) when Tg is very high. There is however no indication in Figure 9 of the time needed to reach the plotted maximum stress state for the different glass transition temperatures - information of great interest when attempting lifetime predictions.

In Figure 10 are plotted the maximum stress levels developed inside of materials with different glass transition temperatures after different amounts of thermal cycling.

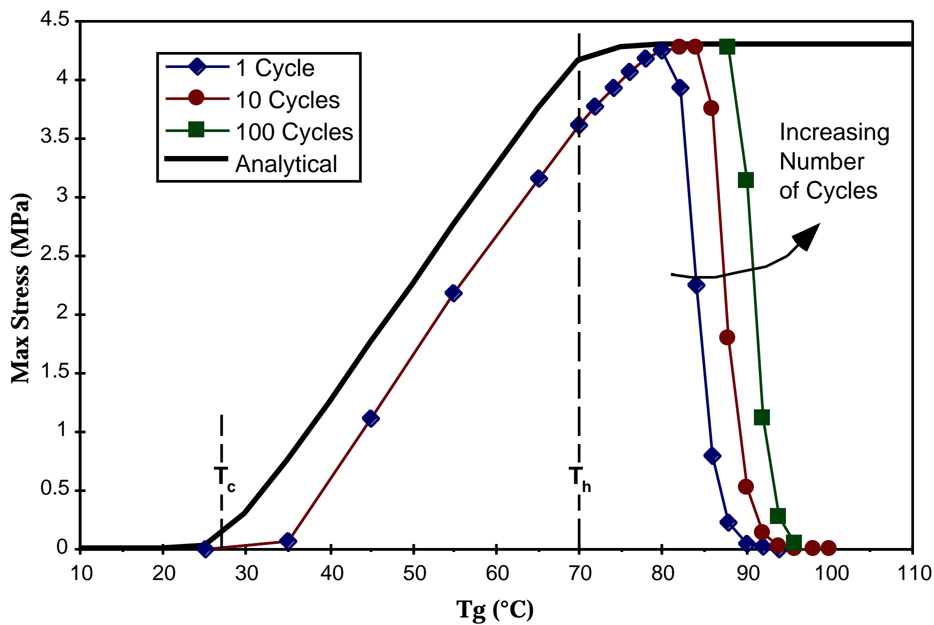

Figure 10. T_g Sensitivity Curve with Cycling Time (cycling between T_c and T_h)

In the figure, four different regions of Tg-sensitivity can be identified, here listed as found on the plot in Figure 10 from left to right:

Region I: Service temperature range exceeds glass transition

In region I, the material is in its rubbery state for the entire span of the cyclic temperature profile. Stress relaxation occurs very quickly in viscoelastic materials at temperatures above the glass transition. Residual stress converges to its maximum value within one cycle, but at no point is that maximum a significantly large value. The stresses simply relax too quickly at both the hot and cold temperatures (Fig. 11).

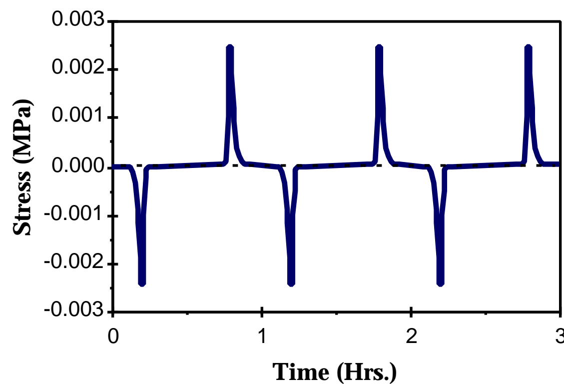

Figure 11. Stress vs. Time for T_g=27°C

Region II: Service temperature range spans the glass transition

In region II, the cycling limits span the transition temperature of the polymer. At the hot temperature relaxation rate is very high, so convergence of stress build-up occurs after only one cycle. Unlike in region I, the material now becomes glassy during cooling to the cold temperature, allowing some of the stress relaxation at the hot temperature to be frozen in as tensile stresses at the clod temperature (Fig. 12).

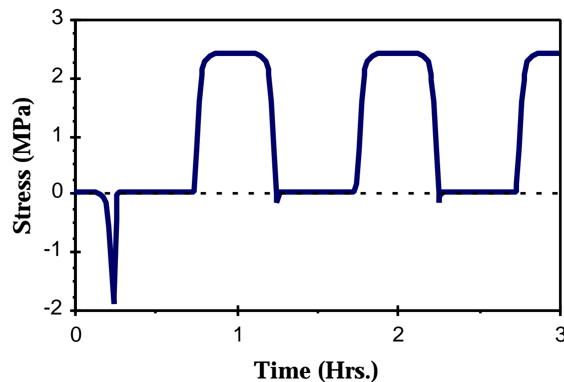

Figure 12. Stress vs. Time for T_g=57°C

Region III: Service temperature range slightly below T_g

In region III, the material is glassy for the entire cycling span. However, the hot temperature is close enough to the glass transition that relaxation rate is high enough to allow for slow relaxation of stresses over many cycles. Tensile residual stresses gradually accumulate (Fig. 13) to the maximum stress value predicted by simple analysis of thermal stresses in the glassy polymer.

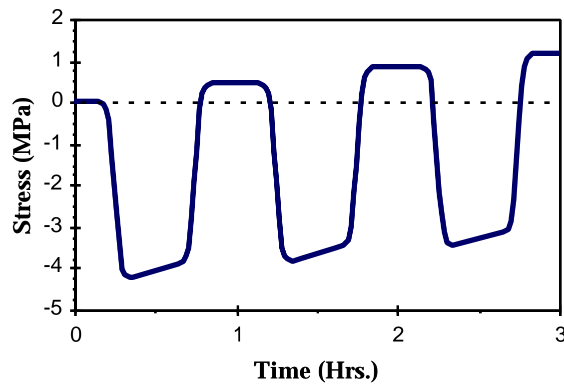

Figure 13. Stress vs. Time for T_g=87°C

Region IV: Service temperature range well above T_g

Like in region I, stress buildup in this region is inconsequential (Fig. 14), but the reason is different. The hot temperature for cycling falls so far below the glass transition region that only a small amount of stress build-up has taken place during the entire lifespan of the application of interest. Where this region begins will depend upon the intended lifetime of the application. For example, for an application that is limited to a lifetime of fifty cycles, region IV would include all Tg's above 92°C.

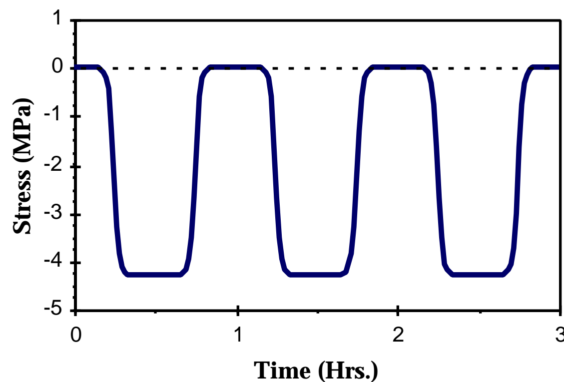

Figure 14. Stress vs. Time for T_g=117°C

3.6 Thermal Profile Sensitivity

The data points produced by the recursive equation are found to match the analytically-derived equation closely in regions I and IV, but diverge greatly for any T_g in between (Fig. 9). This is not surprising since the numerical method accounts for the possibility of relaxation during thermal ramping, where the analytical method assumed near-instantaneous ramping. Cooling polymers slowly will results in reduced residual stress levels; as the temperature is reduced and residual stresses begin to develop in the system, there is more time for relaxation at the accelerated rates of the higher temperatures. The same principle would presumably apply for thermal cycling. A thermal profile with rapid temperature changes would ultimately induce higher residual stresses more quickly than a profile with slower thermal changes. Figures 15 and 16 depict the predicted stress evolution given two different thermal profiles; the Tanh-wave defined by equation 17 and a sine wave with the same amplitude and period.

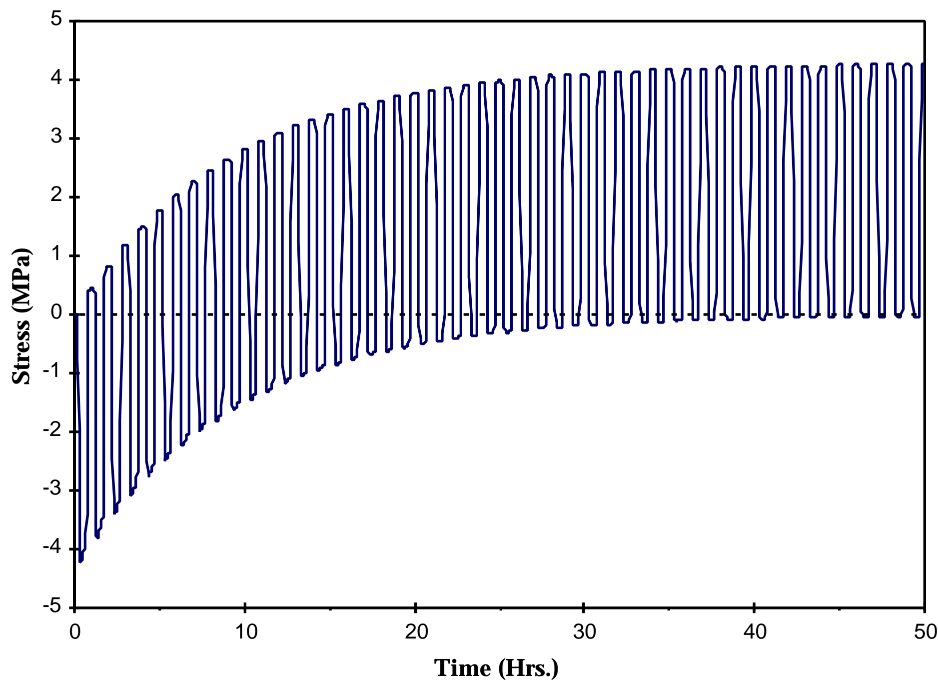

Figure 15. Stress development - Tanh wave

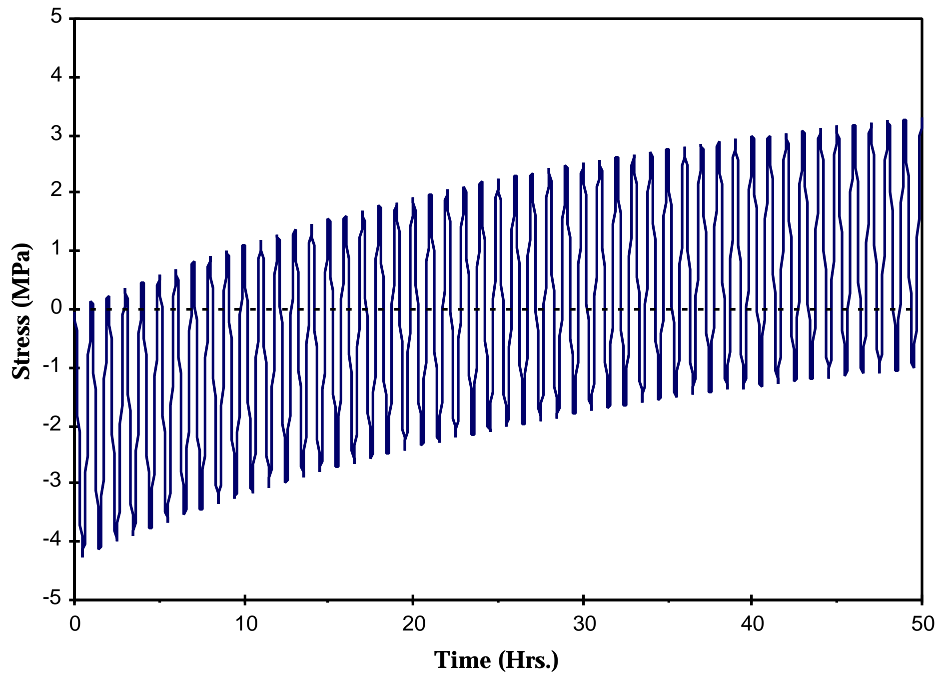

Figure 16. Stress development - Sine wave

The stresses are clearly rising more slowly in Figure 15 than in Figure 16. In addition, the maximum stress level was predicted to be about 2.5% lower - 4.18 MPa as compared to 4.27 MPa for the near-square wave input. In order to reveal the effect of thermal ramp rate on maximum stress level, a number of recursive solutions were again run, this time varying the steepness of the thermal ramp by defining the Tanh-wave as before, but changing the denominator of the hyperbolic functions:

$$T(t) = 27 + 21.5 \quad \mathrm{Tanh}\left[\frac{t-900}{c}\right] - \mathrm{Tanh}\left[\frac{t-2700}{c}\right] \qquad [25]$$

Up to this point, c has been 120. Decreasing c makes the temperature changes steeper; a plot of the results is found in Figure 17.

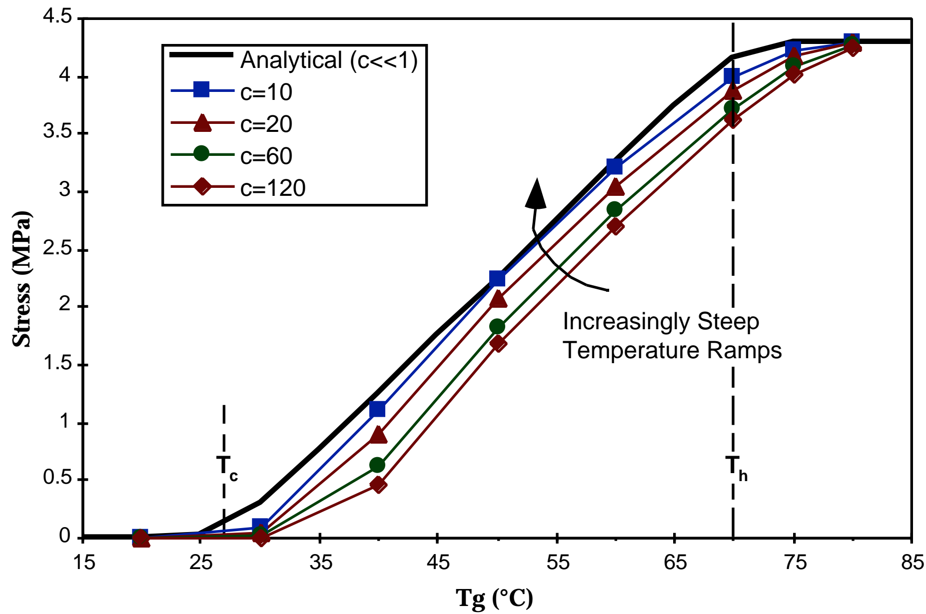

Figure 17. T_g Sensitivity Curve for Different Thermal Profiles

It was found that steeper thermal profiles have more severe maximum stresses, especially in region II, but also to some extent in region III. The smaller the parameter c, the closer the thermal profile is to a square wave, and the closer the stress values come to the analytical equation for maximum stress prediction (equation 24). For problems where operating range spans or nears the glass transition of a material, the particular shape of the thermal profile could be a significant consideration.

Chapter 4 - Finite Element Solution

4.1 The Mesh

The more realistic 2-D geometry of an adhesive layer bonded between two substrates was analyzed using a finite element mesh and the software package ABAQUS. The mesh (Figure 18) was comprised of two layers of 35 eight-node parabolic elements each, with the two layers sharing nineteen nodes at the interface. The top layer was assigned to model a viscoelastic adhesive and the bottom layer was assigned to model an elastic substrate. The layers were made to have equal thickness to facilitate meshing. Plane stress conditions were assumed.

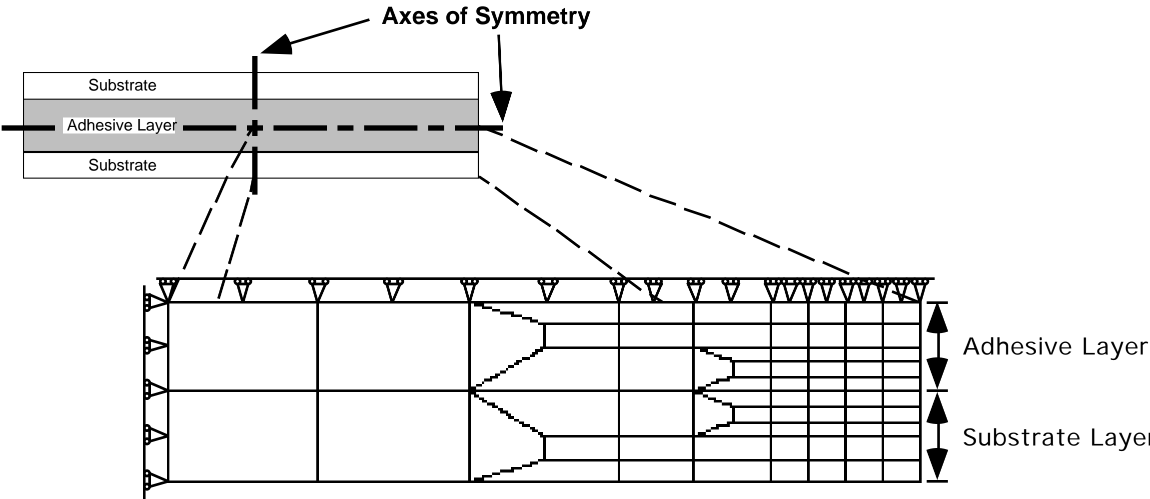

Figure 18. 2-D Finite element mesh of one quarter of a sandwich geometry

The boundary conditions applied to the mesh (included in Figure 18) were selected to enforce symmetry conditions. The axes of symmetry for the mesh are along the left and top boundaries; axial displacement is constrained along the left and transverse displacement is constrained along the top. By enforcing proper symmetry conditions at the boundaries, a mesh representing one fourth of the bond can adequately model the entire 2-D geometry.

ABAQUS is capable of evaluating stress development over time in systems containing viscoelastic elements by time stepping in a manner similar to the previous method. This involves evaluating the full 2-D stress solution for the mesh at hundreds or thousands of time steps per cycle. The mesh was therefore chosen to be relatively coarse to minimize the processing load on the computer. Mesh density is not expected to affect the accuracy of the stress values near the left end of the mesh, where stresses are expected to be nearly constant. Where high gradients

would be expected (near the right end), the stress magnitudes are not expected to be entirely accurate because of the coarseness of the mesh. Nonetheless, useful information can be gleaned from the results by observing the how stress levels in these elements change over time due to thermal cycling.

4.2 ABAQUS results

The finite element analysis was run using the same material properties for the adhesive as in the previous example (section 3.3). For the substrate, modulus of 73 MPa and CTE of 25×10^{-6} $°C^{-1}$ were used. Figure 19 depicts the axial stress profile results returned by the finite element analysis after five temperature cycles.

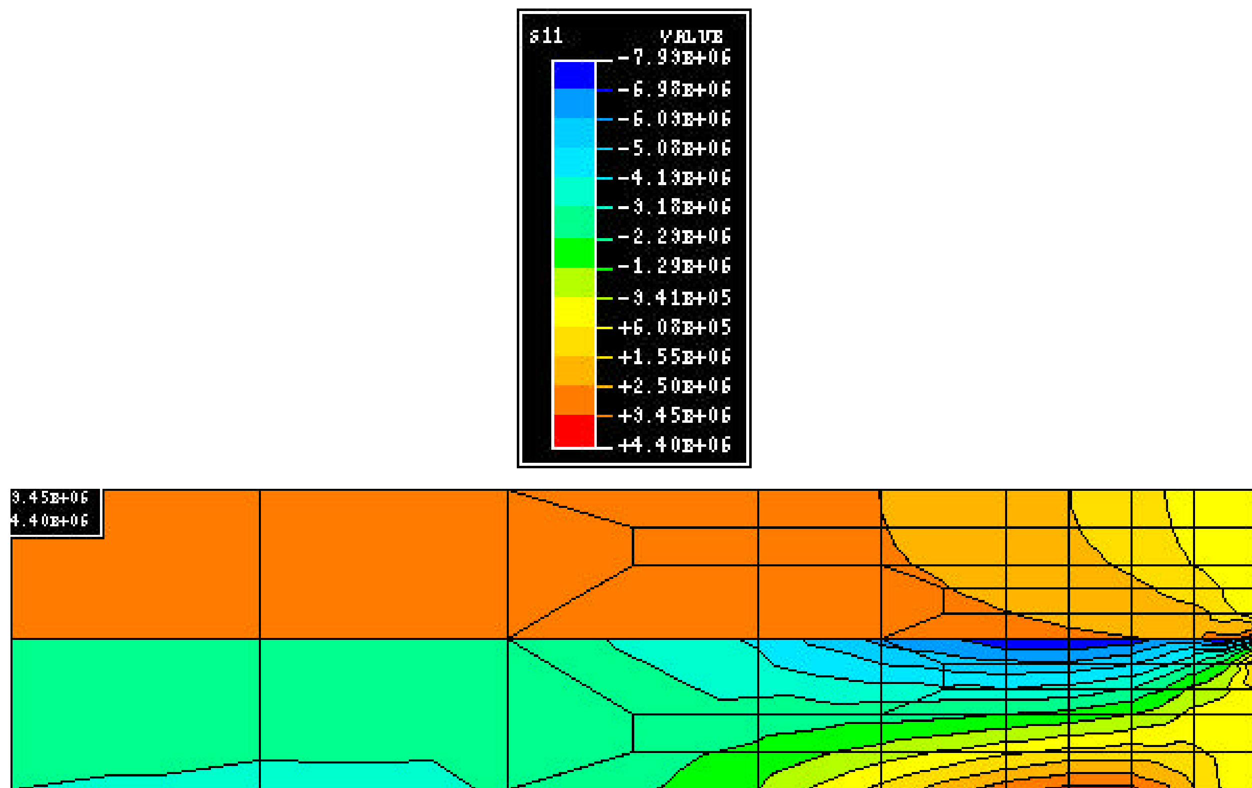

Figure 19. Axial Stress Distribution after Ten Cycles

Axial stress is nearly constant near the left end of the mesh (the axis of symmetry), and falls away to zero at the right side (the free end). Residual axial stress development in the 2-D geometry was found to follow the same trends as predicted by the 1-D analysis. The tensile stresses at the cold temperature were found to increase over the number of cycles due to stress

relaxation at the high temperature. The rate of stress development was nearly the same as predicted by the 1-D solution, similarly nearing steady-state conditions in 50 cycles.

One would expect the high axial stress gradients near the free end to be coupled with significant shear and peel stresses. Where axial stress is nearly constant (away from the free end), both shear and peel stresses should approach zero. The finite element results confirmed these suspicions (Figures 20 and 21). Peel and shear stresses are localized near the end - where a crack is most likely to begin.

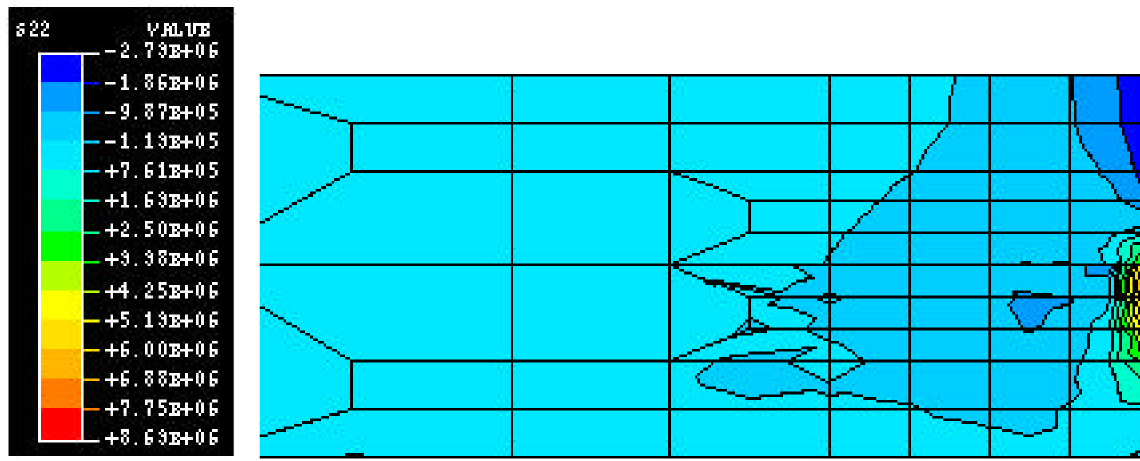

Figure 20. Peel Stress Distribution after Ten Cycles (free end of specimen)

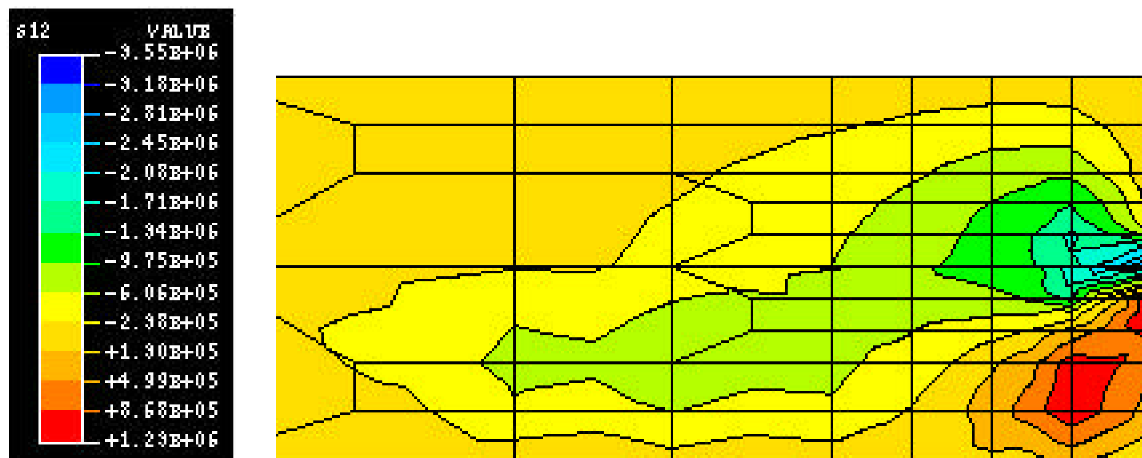

Figure 21. Shear Stress Distribution after Ten Cycles (free end of specimen)

Incremental build-up of shear and peel stresses along the interface at the free end were found to incrementally increase in the same manner as the axial stresses (Figures 22 and 23); indeed, this is a requirement to preserve static equilibrium.

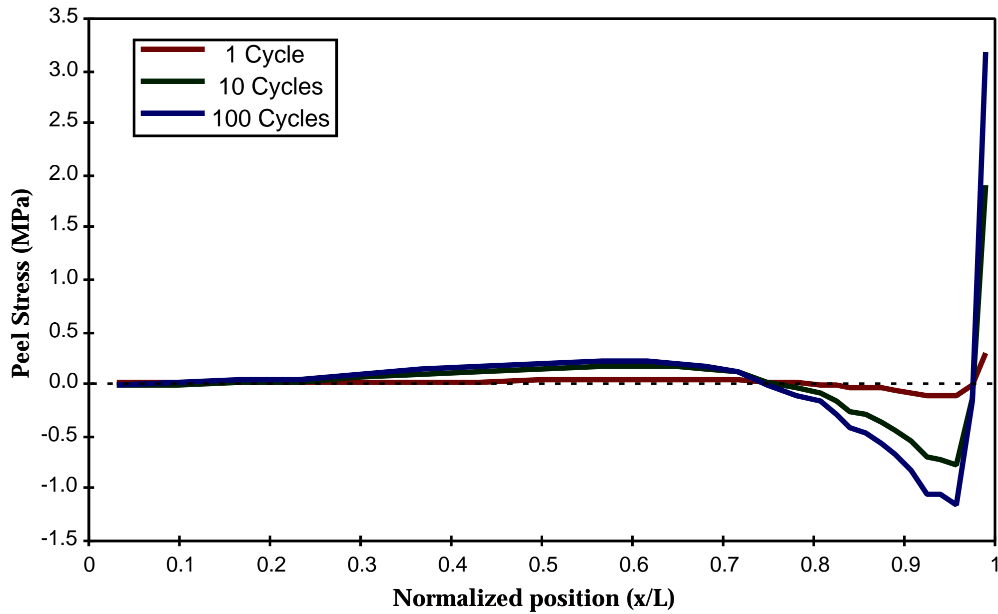

Figure 22. Peel Stress Distribution (Cold Temp.) for Increasing Numbers of Thermal Cycles

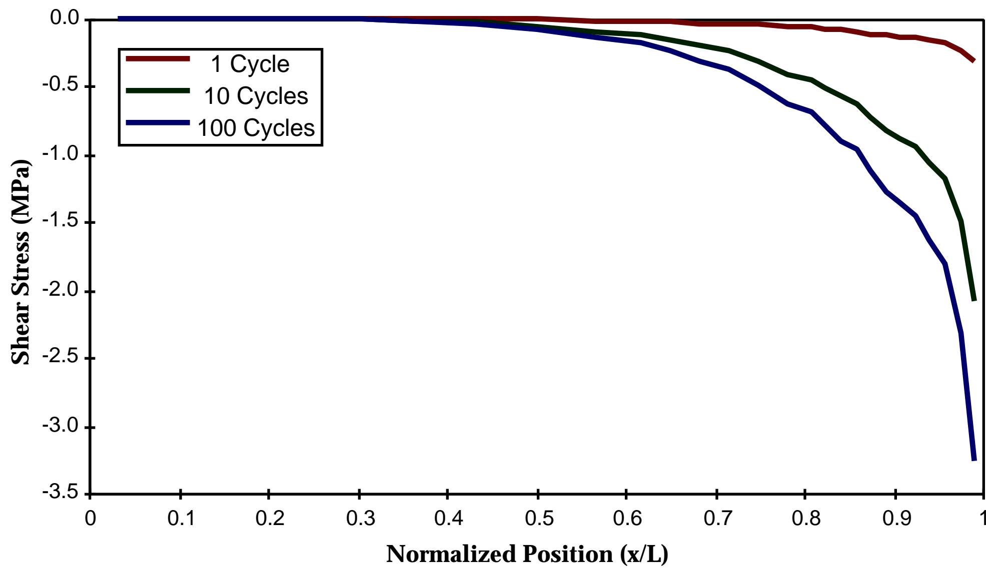

Figure 23. Shear Stress Distribution (Cold Temp.) for Increasing Numbers of Thermal Cycles

The fact that the development is toward greater tensile peel stresses is of critical importance. Tensile peel stresses would be expected to contribute to crack initiation and propagation that has been observed experimentally.

Chapter 5 - Comparison of 1-D and 2-D Analysis Results

In the middle region of an adhesive bond, the adhesive layer is completely constrained by the substrates; stress is uniaxial and effectively independent of position in the bond. Recall that assuming uniform uniaxial stresses was the simplification that allowed for the derivation of the recursive equation in Chapter 3 (equation 12). The 2-D differs from the 1-D case in that total strain in the polymer is not constrained to zero as assumed in the 1-D analysis, but is instead constrained to the thermal expansion of the substrate.

In order to correlate the 1-D and 2-D solutions, we must recall the equation for total strain in a body (equation 3)

$$\varepsilon = \varepsilon_M + \varepsilon_T .$$

Substituting in the thermal expansion of the substrate (ε_T^s) for total strain and the thermal expansion of the polymer (ε_T^p) for thermal strain, we can solve for mechanical strain:

$$\varepsilon_M = \varepsilon_T^s - \varepsilon_T^p = -\int_{T_0}^{T} [\alpha^p(T) - \alpha^s]\, dT \qquad [26]$$

By subtracting the CTE of the substrate (α^s, assumed to be independent of temperature) from the CTE of the polymer in the 1-D analysis, we should be able to get a solution for stress in the center of the bond in the 2-D case from the recursive equation. One consequence is that thermal and residual stresses will be reduced when the difference between CTEs of the adhesive and substrate are reduced, and increase when the difference is increased. If the CTEs ever match exactly, no thermal stresses will be induced in the system.

The axial stress was predicted to be 3.21 MPa using this technique with the 1-D recursive equation, very close to the 3.22 MPa value returned by the 2-D finite element plane stress solution. The 1-D equation is indeed sufficient to predict axial stress development in the center region of adhesive bonds and can be applied in place of the more complicated and time-consuming finite element analyses.

Chapter 6 - Fracture Analysis

Let us consider one half of the bonded sandwich geometry described above after it has undergone some thermal cycling. The solutions presented in previous chapters predict a resulting tensile residual stress state in the polymer layer (when the polymer CTE exceeds the substrate CTE at the hot temperature). Strain energy release rate for the system can be derived using energy balance methods.

We will assume that symmetric, sharp pre-cracks exist at each of the interfaces at the free end (Figure 24). We will also assume any crack propagation will occur simultaneously and identically at both interfaces, and that the two interface cracks will always be of uniform length through the width of the system.

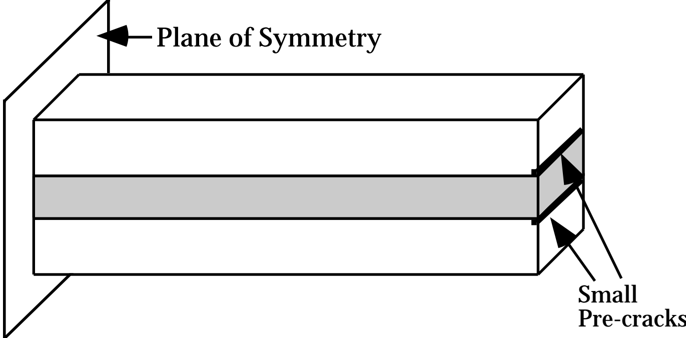

Figure 24. Half of sandwich with pre-cracks at end

Stored strain energy (U) in a material with arbitrary elastic behavior subjected to a general state of stress is determined by integrating the stress ( ) with respect to strain ( ) through the volume V [23]:

$$U = \int_V \left[\int_0^{\varepsilon_{ij}} \sigma_{ij} d\varepsilon_{ij} \right] dV \qquad [27]$$

For an isotropic, linear-elastic, material, the expression becomes:

$$U = \int_V \left[\frac{1+\nu}{2E} \sigma_{ij}\sigma_{ij} - \frac{\nu}{2E} \sigma_{ii}^2 \right] dV \qquad [28]$$

where E is modulus and is Poisson’s ratio.

The total stored strain energy (U_{tot}) in the bonded system is:

$$U_{tot} = U_a + 2U_s \tag{29}$$

where U_a and U_s are the total strain energies stored in the adhesive and substrate layers respectively, as evaluated by equation 27.

Let us consider strain energy in the substrates in view of the equilibrium of stresses in the system. In the direction perpendicular to the bond, the substrates will not sustain much stress; free surfaces exist on top and bottom. Parallel to the bond the substrates will sustain some stress, quantifiable by considering a simple force balance at a cross-section of the sandwich (Fig. 25):

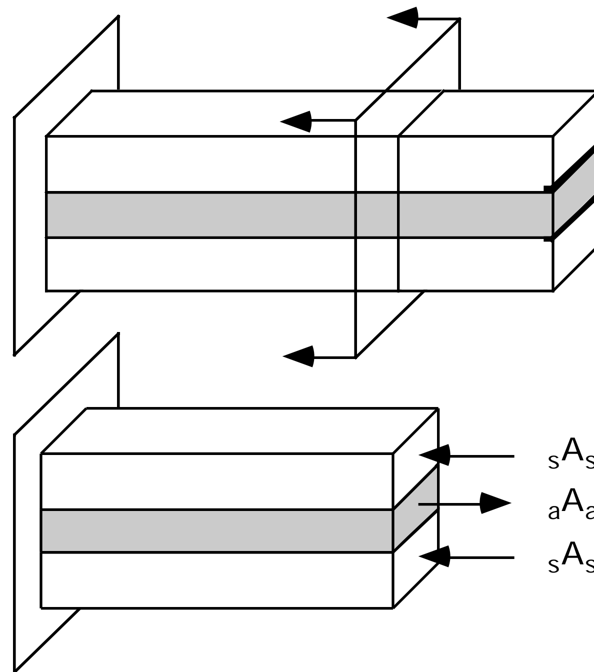

Figure 25. Sandwich geometry cross-section

It follows from static equilibrium that the magnitude of the tensile force in the adhesive layer is equal to the total compressive force in the substrates

$${}_aA_a = 2 \quad {}_sA_s. \tag{30}$$

Assuming uniform width, the stress in the substrate will equal to stress in the adhesive layer times one half of the ratio of thicknesses:

$$_{s} = \frac{1}{2} \quad _{a} \frac{h}{H} \qquad [31]$$

where h is the adhesive layer thickness and H is the substrate layer thickness.

For a typical bond with a thin adhesive layer as compared to the substrates (h/H << 1), stress in the substrates will be very small. Strain energy in a body is proportional to the square of the stress, so the greater the thickness of the substrate relative to the adhesive, the less strain energy stored in the adhesive. Strain energy is also inversely proportional to modulus; for the case of a typical metal-polymer bond, substrate stiffness is at least an order of magnitude greater than adhesive stiffness. Given these "thin-bond line" and "stiff-substrate" conditions, the contribution of the substrates in the total stored strain energy equation 29 is insignificant. The expression for total stored strain energy in the system now becomes:

$$U_{tot} \quad U_{a} \qquad [32]$$

where U_a is evaluated using equation 27.

If the interface cracks propagate a finite distance a, the strain energy in that portion of the bond is released. Equation 27 is difficult to evaluate in the region near the free ends where the crack grows; stress gradients are high, complicating the integrals. However, consider a bond that is "relatively long". Stress gradient zones at the free end do not extend close to the center (Figures 19-22). Debonding does not cause a significant change in stress magnitudes or distributions; the bond is simply becomes shorter. For such a long bond, total strain energy remaining after a crack grows a finite distance a (Figure 26a) is exactly equivalent to the strain energy stored in a bond a shorter in length(Figure 26b).

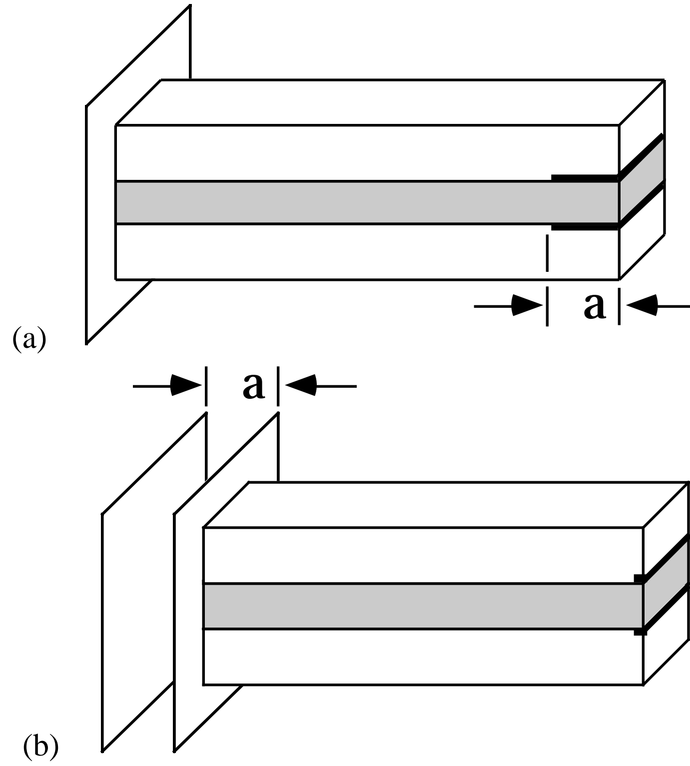

Figure 26. Sandwich geometries with equal stored strain energies

(a) Sandwich of length l containing cracks of length a. (b) Sandwich of length l- a

Energy release is therefore equivalent to the stored strain energy in any a-long segment of the bond which is well away from the crack tip. We choose to consider a segment from the center of the bond, where we know that normal stresses will be constant and uniform, and shear stresses will be zero. Strain energy in such a piece is simply evaluated; equation 27 becomes a simplification of equation 28:

$$U = V * \frac{1}{2E}\left({}^{2}_{xx} + {}^{2}_{yy} + {}^{2}_{zz} \right) - \frac{}{2E}\left({}_{xx}\;{}_{yy} + {}_{yy}\;{}_{zz} + {}_{xx}\;{}_{zz} \right) \qquad [33]$$

where V is the volume of the segment (adhesive only).

Applied strain energy release rate (denoted G, or abbreviated SERR) is a measure of energy per unit surface area that would be released by crack propagation. It is the most useful measure of strain energy in a bond to consider, because it can be compared to the experimentally-determined critical value for a given system. The critical strain energy release rate (G_c) for a system is a measure of the minimum energy required for crack growth. The strain energy release rate is simply derived; stored strain energy (equation 33) is divided by the new area created along each of the fracture surfaces. This yields:

$$G = \frac{h}{4E}\left[\left({}^{2}_{xx} + {}^{2}_{yy} + {}^{2}_{zz}\right) - \left({}_{xx}\,{}_{yy} + {}_{yy}\,{}_{zz} + {}_{xx}\,{}_{zz}\right)\right] \quad [34]$$

Recall again that we have ceased considering the contribution of the substrates, so all variables in the equation refer to the adhesive layer only.

Simplification of equation 34 for particular adhesive bond geometries will yield different results. Presented here are two different cases; it will be left to the reader to decide which (or what combination of the two) is most appropriate for any particular geometry of interest. In all cases, s is the value of axial stress in the center of the bond and h and E are thickness and stiffness of the adhesive.

Thick, narrow bond - uniaxial stress

A bond that is narrow in comparison to its bondline thickness will have a nearly uniaxial stress field built in by thermal cycling. Across the width of the interface, stresses will not develop significantly because the stress-free edges are close and the adhesive will neck in response to Poisson contraction from the axial stresses. Peel and shear stresses will be concentrated only at the ends. The recursive solution in Chapter 3 was such a problem; only stress in the axial direction was non-zero. For the uniaxial stress case, equation 34 reduces to the simple form:

$$G = \frac{h}{4E}\;{}^{2} \quad [35]$$

Thin, wide bond - equal biaxial stresses

A bond which is long and wide in comparison with its thickness will have equal residual biaxial stresses built in by thermal cycling. Because the bond is thin and wide, the adhesive cannot neck and stresses can develop across the width of the bond in the same manner as along the length. As with the thick, narrow bond, peel stresses and shear stresses will be concentrated in small regions near the edges.

When debonding occurs, the length of debonded region relative to thickness will determine the proper expression for G. When the debond is relatively short, the debonded region is under plane stress conditions, and hence still sustains stress in the transverse direction. The proper simplification of equation 34 is the same as above; only strain energy stored in the material by axial stresses has been released, so equation 35 will be sufficient to describe G. When the debonded length is much longer than the material is thick, energy stored in the material by transverse stresses can be released as well; the G equation becomes:

$$G = \frac{h\left(1 - \ \right)}{2E} \quad ^2 \qquad [36]$$

A thin, wide bond with a relatively long crack will have greater G-values than the thick, narrow bond for a given stress level.

The strain energy release rate for a layered geometry test specimen (Notched Coating Adhesion or NCA specimen) which is subjected to biaxial residual stresses and uniaxial mechanical loading has been developed by Chang, et. al. [24]:

$$G = \frac{h}{E}\left\{\left[\left(\ _t + \ _m\right)^2 + \left(\ _t + \ _m\right)\ E\right]\left(1 - \ \right) + \tfrac{1}{2}\left(\ E\right)^2\right\} \qquad [37]$$

where $_t$ is thermal residual stress, $_m$ is residual stress from moisture swelling, and is applied strain. For a layered geometry with no loading outside of built-in thermal residual stresses, applied strain and swelling stresses are zero. The equation simplifies to:

$$G = \frac{h\left(1 - \ \right)}{E} \quad ^2 \qquad [38]$$

which is double the equation for G of the sandwich geometry under biaxial stress loading (equation 36). This makes intuitive sense, as the same amount of strain energy is released from the polymer layer, but only half as much new surface area is created as for the sandwich geometry.

To this point, the equations derived have expressed G as a function of stress. However, if we can express stress as a function of G, then testing for G_c of a system would allow us to quantify residual stress build-up in subsequent specimens from the change in critical applied strain. For example, manipulating equation 37 yields:

$$= \frac{_cE}{2}\ \sqrt{\frac{4G_c - \left(1 + \ \right)\ _c^2Eh}{\left(1 - \ \right)\ _c^2Eh}} - 1 \qquad [39]$$

We first test an unconditioned specimen to get a reference G_c. Testing a series of NCA specimens, each having first undergone a different amount of thermal cycling, would then yield an experimental data set for stress development over time.

A similar study was completed numerically using a finite element code originally written by Chang for analysis of NCA specimens. The ABAQUS program calculates the J-Integral around a path enclosing a crack in a layered NCA specimen, calculating the strain energy release rate for any applied strain. The code was modified by the author to include viscoelasticity, thermal dependence, and an applied thermal profile like that used in chapter 4.

The finite element study calculated SERR of an NCA specimen for twelve different cases: four different applied strains ( ) on each of three specimens - with 27°C - 70°C thermal cycling for zero, ten, and one hundred cycles. Figure 27 contains data from this finite element study plotted with curves depicting the uniaxial plane stress analytical solutions; applied strain energy release rate is plotted against applied strain. The individual data points are the strain energy release results returned by the finite element code. Each curve depicts G for a uniaxial stress case (equation 35), where stress is defined:

$$= {}_t + {}_o \qquad [40]$$

Total stress is the sum of the stresses from thermal cycling and mechanical loading. The values of residual thermal stress ($_t$) used in the analytical solutions were taken from the results of the FE solutions; the axial stress near the fixed end of the model was used.

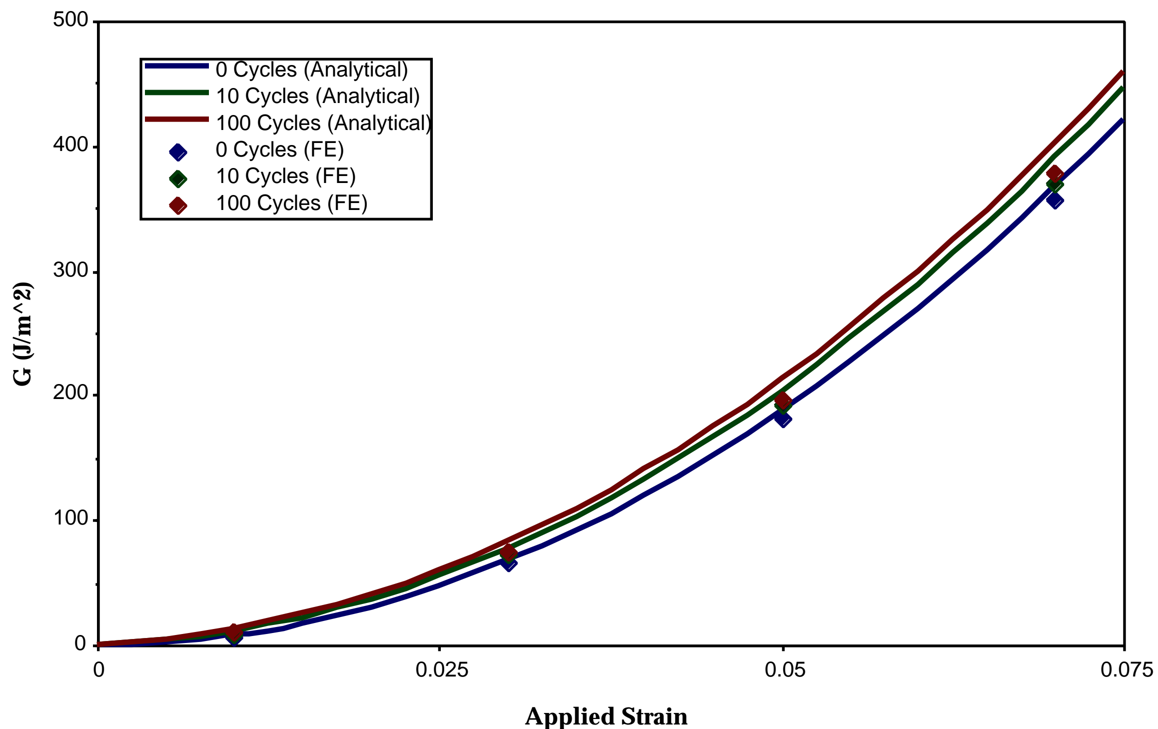

Figure 27. Strain Energy Release Rate for Layered Specimens After Thermal Cycling

Thermal conditioning and the resulting build-up in residual tensile stresses clearly produce an increase in SERR at the crack tip. The FE stress results follow the same trend as that predicted by equation 35, with increasing values over time. The maximum axial stress magnitude (after 100 cycles) returned by the NCA FE analysis was 3.25 MPa, matching the results returned by the previous FE solution and the recursive solution (3.22 and 3.21 MPa respectively). Using the recursive equation together with the appropriate strain energy release rate expression (from equations 35-36) for a given loading could therefore serve as a quick and easy way to calculate the effect of thermal cycling on applied strain energy release rate at the crack tip in an adhesively-bonded system.

Chapter 7 - Discussion of Analysis Results

Given the results presented, a plausible mechanism for the previously described debonding and contraction behavior can be proposed. Initially, the bond is at the cold temperature and the residual stresses are minimal. Raising the temperature of the bond induces a compressive stress in the polymer layer because of the CTE mismatch between the adhesive and substrate. The higher temperature facilitates polymer chain mobility and relaxation of the compressive thermal stress. Cooling the system freezes in the structural changes; relaxation at the hot temperature is reflected in an increased tensile stress at the cold temperature. The low temperature inhibits flow, so the tensile stresses relax only very slowly. The initial stress state cannot be recovered before the next thermal cycle begins; there is now a net residual stress where none existed before. Thermal cycling thereby ratchets up the cold-side tensile stress with each cycle.

Having different initial conditions does not change the results much; if the material is not initially stress-free, it simply starts with some thermal history. The trend of rising residual stresses will still occur, but will take a longer or shorter time to rise to maximum stress magnitude. The same is true if the initial temperature is not the high or low temperature. At the low temperature, the material will again start with initial residual stresses, this time from heating/cooling from the initial temperature.

At some point, debonding initiates at the interfaces near the ends of the specimen. Applied strain energy release rate at the tip of an interface crack in the bond has been shown to increase from thermal cycling as a result of increasing residual stresses. However, to determine exactly when and how a crack is propagated for a given system, we must know the fracture toughness of the material as a function of temperature. Stresses and strain energy release rate are highest at the cold temperature, suggesting that crack propagation could occur when the system is coldest. Based on the work of Gorce, et. al. [25] however, it seems unreasonable that cracking would occur in polyurethanes when very cold; polyurethane toughness was found to rise dramatically as temperature dropped. Probably crack growth in polyurethane bonds occurs during the thermal ramping, at a temperature between the maximum and minimums at which tensile stresses are of significant magnitude but toughness has not yet become very high.

Once released from its constraints by debonding, the polymer layer contracts. Contraction occurs as the material returns to its stress-free strain. The change in stress-free strain from the initial condition is a result of viscoelastic flow that occurred in the polymer while under compressive stress at the hot temperature of each cycle. It is evidenced by the increased tensile stress level at the cold temperature.

The magnitude of changes in residual stress state at an adhesive interface are expected to be more serious under certain conditions. A summary is presented in Figures 28 and 29.

Rate of Stress Development	
Faster	**Slower**
Lower Characteristic Relaxation Time	Higher Characteristic Relaxation Time
Hot Temperature Closer to Glass Transition	Hot Temperature Further from Glass Transition
Steeper Thermal Ramps	More Gradual Thermal Ramps
Longer Time at Hot Temperature	Shorter Time at Hot Temperature

Figure 28. Details affecting rate of stress development

Magnitude of Maximum Stress	
Higher	**Lower**
Higher Between Materials	Lower Between Materials
Greater T	Lesser T
Higher Tg (if spanned by temperature range)	Lower Tg (if spanned by temperature range)
Steeper Thermal Ramps	More Gradual Thermal Ramps
Plane Strain	Plane Stress
Viscoelastic Fluid	Viscoelastic Solid
Higher Material Stiffness	Lower Material Stiffness

Figure 29. Details affecting maximum magnitude of built-in stresses

Figure 28 lists the effects of different parameters on the rate of stress development. Figure 29 summarizes the effects of different parameters on the magnitude of the built-in residual tensile stress.

Chapter 8 - Experimental Verification

The author has attempted to experimentally verify the hypotheses and numerical results presented to this point. A polyurethane-aluminum system was selected based on the fact that spontaneous debonding and contraction due to thermal loading had reportedly been observed in industry. The course for the experimental verification attempt was set as follows.

8.1 Strategy

The component materials were first to be characterized. Stiffness and thermal expansion of the aluminum was already well-documented and easily verified. The properties of aluminum were assumed to be constant over the temperature range of interest (-50°C to 150°C).

A number of different techniques were to be employed to characterize the thermal and mechanical properties of the polyurethane adhesive. Differential Scanning Calorimetery (DSC) would be used both to determine the Tg and to ascertain if any irreversible chemical changes were taking place during heating. Thermal Mechanical Analysis (TMA) would be used to measure the coefficient of thermal expansion of the polyurethane as a function of temperature. Dynamic Mechanical Analysis (DMA) would be used to measure the storage and loss modulii as functions of temperature.

The fracture toughness of polyurethane was to be measured using static double cantilever beam (DCB) tests, conducted both at room-temperature and sub-ambient temperatures. The fatigue toughness of the PUR was also to be measured using DCB specimens tested under fatigue loading. Fatigue loading was an important consideration because cracks have been found to propagate through materials due to fatigue at loadings one-tenth of their fracture toughness [26].

Once the data had been used to help select the appropriate constants for a Maxwell mechanical model, the previously described computational methods could be used to make predictions to compare to experimental observations. The recursive equation developed previously could be used to predict axial stress development in the bond for any given thermal profile. More detailed finite element analyses could be used to predict strain energy release rate for particular bond geometries. These strain energy predictions would be compared to static and fatigue DCB fracture data, from which predictions could be made of expected crack growth rates. Experimental observation would then confirm or repudiate both the hypothesized role of built-in residual stresses in crack growth and the methods proposed to predict said stresses. If the proposed analytical and numerical methods can be verified, they could prove useful tools for adhesive bond durability study and design.

8.2 Procedures

The adhesive selected was a two-part polyurethane elastomer made with a variant of Dow's Voranol polyol and a methylene diphenyl diisocyanate (MDI). It is a polyether cross-linked soft-segment matrix with suspended MDI aggregate hard segments. At room temperature, the soft segment is rubbery and the MDI acts as a stiffening glassy backbone.

The polyurethane was made by mixing the isocyanate and polyol together in a weight ratio of 71 to 100. Generally, the polymer was made in 40 g batches. Good mixing of the two components required stirring briskly by hand for 15-20 seconds. Care was taken to scrape the sides of the mixing cup during stirring. Handling time before the onset of cure was restricted to 120 seconds, with seven days at room temperature recommended for full cure.

The polyurethane was bonded between aluminum substrates 1" wide, 8" long, and 0.25" thick. The substrates were first pretreated with a sodium-hydroxide etching process to insure consistent surface characteristics from one specimen to another. This procedure is commonly utilized by the chemists at Virginia Tech and was recommended by Dr. John Dillard [27]. It first required hand-scrubbing, grit-blasting, and ultrasonic cleaning of the aluminum. The substrates were then submerged in a 5 weight-percent NaOH-H_2O solution for three minutes, rinsed with purified water, submerged in a 50 volume-percent nitric acid bath, and rinsed again with purified water. The specimens were allowed to dry in air for 24 hours before being used.

Bonded specimens were cast in a silicon rubber mold to prevent spillage out the sides before the PUR set. First, one aluminum substrate was placed in the mold. Bond thickness was set using spacers at each end; a 0.007"-thick layer of tape for DCB specimens and a .0625" to .25"-thick piece of Teflon for NCA specimens. After the PUR was poured, the top substrate was placed over the bond (aluminum for DCBs, Teflon or acrylic for NCAs). Care had to be taken to lay the top over the bond correctly, placing one end completely down first and then slowly lowering the other into place. In this way we attempted to minimize the possibility that air pockets would be trapped underneath. The ends were lightly pressed down to insure any excess adhesive was squeezed out of the bond. Specimens were allowed to cure for at least one day in the mold, and were then removed and allowed to cure an additional six days outside of the mold. Curing took place at room temperature.

Fracture testing was performed on double cantilever beam (DCB) specimens in an Instron 4500 screw-driven loading frame. The testing procedure used was a standard quasi-static DCB test, with compliance-method analysis. A comprehensive description of the method and analysis along with consideration of loading rate effects can be found in reference 28. The critical strain

energy release rate for each loading cycle was taken to be the point at which the crack arrested. Normally, an average of three cycles would be run on each specimen, all with crack readings at least 50 mm away from either end.

Sub-ambient testing was performed by mounting a Thermotron environmental chamber inside the Instron. Liquid nitrogen was used as the coolant. A fan was set above the chamber to blow air over the grip shaft where it protruded from the chamber in hopes of inhibiting cooling of the load cell itself. Specimens were left in the chamber for at least 30 minutes before testing to insure that they were thermally equilibrated. During testing, the door to the chamber would periodically be opened briefly to make crack measurements.

8.3 Problems And Solutions

A number of problems were encountered while attempting to make good adhesive specimens with polyurethane.

8.3.1 Problems With Mixing

Considerable bubbling and foaming was noticed in the initial samples. One reason was that air bubbles were introduced into the system during hand-mixing. A hand-held static-mixing dispenser was made to eliminate this problem, but was found to inadequately mix the adhesive. Eventually it was determined that centrifuging the PUR after stirring was a good method to remove any air bubbles mixed into the adhesive.

Foaming was still a problem in samples that had been centrifuged. Foaming occurs in polyurethanes that are contaminated with water; the water reacts with isocyanate to form CO_2 during curing, foaming the adhesive. A rotovap was used to remove any water that might have been suspended in the polyol, reducing but not eliminating the foaming problem. It was later determined that the ambient humidity alone was high enough to cause PUR curing in air to foam. The entire mixing process was thereafter performed in a glove box with a controlled N_2 environment and a maximum of 30% relative humidity at the recommendation of Dr. Tom Ward [29].

8.3.2 Problems With Cure Time

The onset of cure was reported to be 2 minutes, making it a limiting factor in specimen production. However, over the months of making samples, cure time was found to fluctuate significantly. The most significant difference found was due to changing temperature. A rise in

room temperature of as few as 5 degrees Celsius due to the building heaters activating was responsible at one point for the PUR curing too quickly to make specimens. Cure was so fast that after 15 seconds of mixing, heat from the exothermic reaction could already be detected. In addition, different formulations of the PUR were tried and were found to have different gel times. Because the mixing, centrifuging, and molding process required at least two minutes, any significant curing before that point was impossible to deal with.

8.3.3 Problems With Consistency

After debugging the specimen-making process, it seemed that enough familiarity with the material had been gained to begin to make specimens regularly. These specimens were still found to contain a few small bubbles (presumably from the specimen casting process), but no foaming was occurring. It would have been optimal to eliminate all bubbling, but no way was found to consistently insure bubbling would not occur. The bubbles in most of the specimens seemed to be of consistent density; it was hoped that that any effects of bubbling on the mechanics would be similarly consistent.

8.4 Experimental Results

Experimental data acquired by testing specimens of this material system was extremely inconsistent. TMA testing did not reveal a kinked line form typical of polymers. Differences between first and second sets of DSC and DMA data gathered from a single specimen seemed to indicate irreversible chemical changes occurring during the first heating cycle (see Appendix E, Pages 1-4).

Room temperature DCB testing revealed viscoelastic flow of the polymer layer during testing. The material response was very time dependent; convergence of the load to a constant value sometimes required over 6 hours. Obvious permanent deformation on some specimens led to the conclusion that energy in the system was being dissipated by flow in the material, raising questions about the accuracy of the data. The excessive amount of bridging that was observed led one to question how the crack tip should really be defined, and how realistic calculations of strain energy release would be if energy was being released in the bridging regions, beyond which the ostensible crack tip was supposed to have progressed.

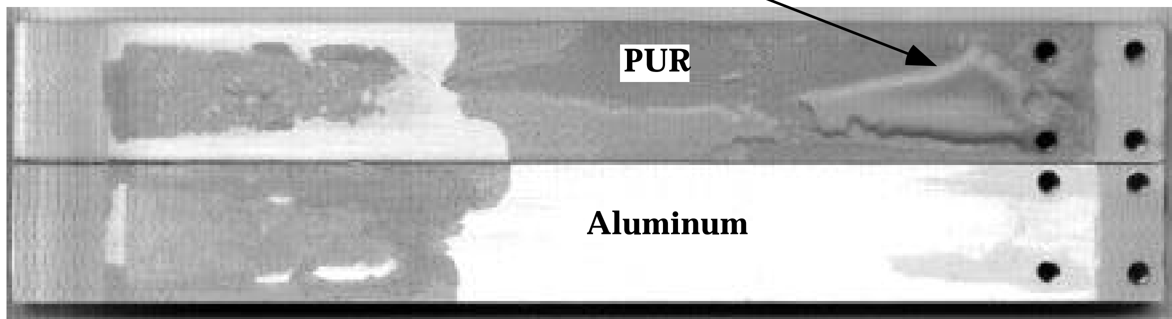

Figure 30. Typical DCB fracture surface from testing at room temperature

DCB testing at -40°C was considered a failure not because of viscoelastic flow, but because the apparent critical strain energy release rate decreased with every cycle. Standard deviation for each data set was 35-50% of the mean value. It was later discovered that the load readings from an unloaded load cell would change with temperature; the cooling chamber and blower alone could change the reading from the load cell by more than 150N in 30 minutes. Sub-Ambient DCBs did have an intriguing fracture surface though; uniform regions along the edges of the specimen fractured very differently than the center regions of the bond.

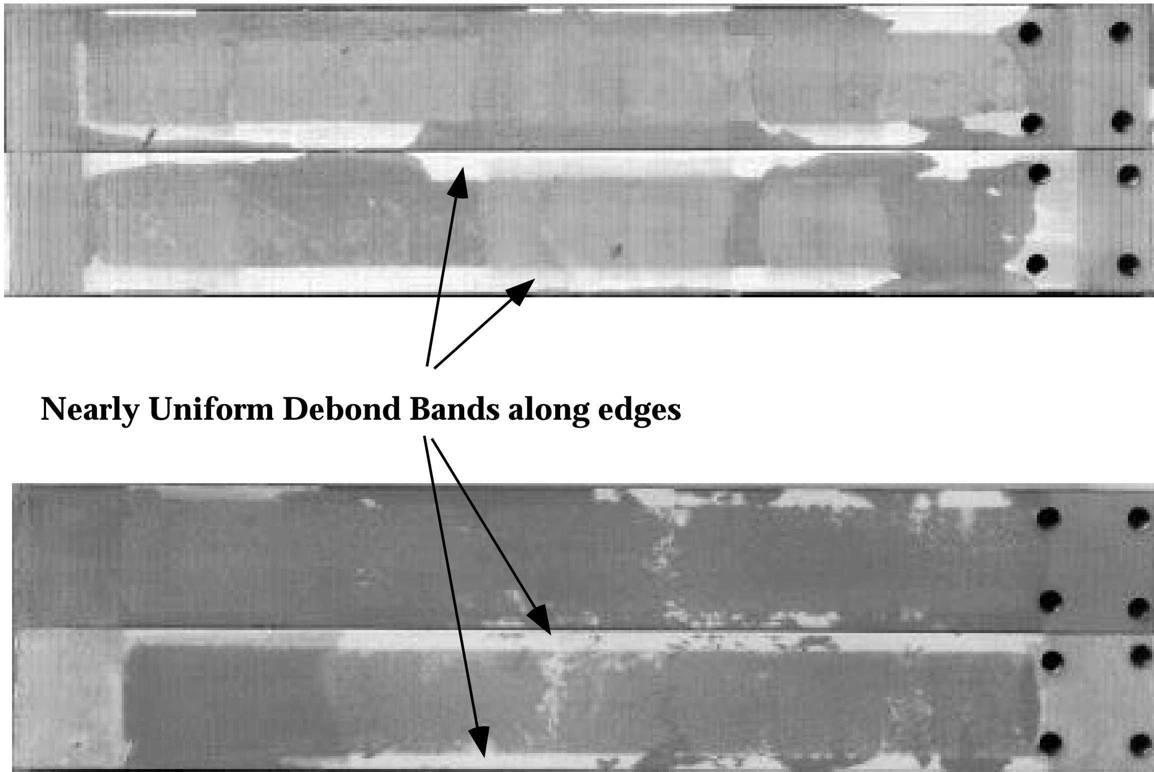

Figure 31. Interesting debonding patterns for specimens tested at -40°C

A number of different theories to explain the existence of these bands were proposed. The bands are perhaps evidence of water ingression from the edges; the water-permeated regions could act much differently when tested under sub-freezing temperatures. Another possible cause is concentrations of tensile peel stresses at the edges. Because the bond is thin (.007"), the thermal stresses in the bond would be equal biaxial, with peel stress concentrations at all free edges. The additional peel stress at the edges could perhaps have promoted the formation of these bands. No definitive explanation of the cause of the phenomenon was developed.

Chapter 9 - Conclusion

Although adhesive applications can be designed with consideration given to particular environmental conditions, it is important to understand that the residual stress state can change significantly over time as a result of viscoelastic flow during thermal cycling in some circumstances. This work has predicted significant stress development in particluar cases for a polyurethane-aluminum bond. However, the incremental stress increase phenomenon is a result of the basic mechanical characteristics of all adhesive bonds: CTE mismatch and a viscoelastic adhesive. The phenomenon should therefore transcend the particular problem presented here, and apply to at least some degree to all adhesive bonds. The speed and severity of the phenomenon will be deterimined by the parameters of each individual problem. Neglecting the potential for residual stress increases due to thermal cycling could result in overpredicting bond durability, resulting in unexpected failures of applications. Thick bonds are especially vulnerable to this potential problem.

A strategy for experimental verification of the numerical results was proposed. An attempt was made to utilize the strategy to verify stress build-up during thermal cycling and identify more precisely the mechanism of debonding in a polyurethane-aluminum bond. Much difficulty was encountered while working with the polyurethane, and good material characterization data was never really obtained. The experimental strategy recommended seemingly remains valid. It is recommended that future experimentation be performed with material systems already very familiar to the reseacher and easy to work with.

This work has developed some tools that could be used to predict the effect of thermal cycling on bond residual stresses and durability. The recursive equation is one method to simply calculate residual stress build-up in a bond given the thermal profile. With stresses known, simple fracture mechanics analysis yields predictions of the increase in applied strain energy release rate as a function of residual stress. It is hoped that these simple tools combined with a greater understanding of the role of viscoelasticity in the mechanics of a bonded joint will eventually lead to more durable design of adhesively bonded applications in the future.

Chapter 10 - Recommendations for Future Work

The future direction of this project should be a full implementation of an improved strategy based on that outlined above for experimental work. This includes:

- selection of an adhesive system to study
- complete characterization of the adhesive
- prediction of stress development from the recursive equation
- verification of residual stress magnitude build-up in layered specimens using NCA testing.
- prediction of crack growth rate from fracture mechanics
- comparison to observed crack growth rates in real specimens
- identification of fracture or fatigue crack growth as the mechanism of failure.

A lot of work outside of the current scope could be added as a next step to enhance the understanding of the problem provided by this project.:

The addition of thermal conduction effects could be an important contribution. While not considered here, the direction from which heat is being applied and the relative thermal conduction coefficients of the components in the joint could have a big effect on the stress magnitudes in the bond. Perhaps the possibility of thermal shock effects would be exposed by such a study.

A reversal of the problem - from considering an adhesive joint to considering a metal layer packaged in plastic would be useful to see how the principles used in the analysis of the bonded problem apply to plastic-packaged components in the electronics industry. Physical aging of materials over long times and the corresponding residual stresses would be another consideration that may be useful to take into account. Often, joints undergo mechanical as well as thermal loading; additions to the recursive equation could be made to take this factor into account.

Thermal profiles are seldom exactly predictable curves; more often, a plot of temperature over time reveals the effects of random distribution. Statistical methods could be combined with the current analysis to develop solutions for systems encountering more realistic thermal profiles.

References

1. Timoshenko, S. P., "Analysis of Bi-Metal Thermostats", *J. Opt. Soc. Am.,* Vol. 11, pp. 233-255. 1925.

2. Erdogan. "Stress Distribution in Bonded Dissimilar Materials with Cracks", *J. App. Mech.*, Vol. 32. pp. 403-410. 1965.

3. Chen, W. T. and Nelson, C. W., "Thermal Stress in Bonded Joints", *IBM J. Res. Dev.,* Vol. 23, No. 2, pp. 179-188. 1979.

4. Suhir, "Stresses in Bi-Metal Thermostats", *J. App. Mech.,* Vol 53, pp. 657-660. 1986.

5. Suhir. "Interfacial Stresses in Bi-Metal Thermostats", *J. App. Mech.,* Vol. 56, pp. 595-600. 1989.

6. Losi, G. and Knauss, W., "Thermal Stresses in Nonlinearly Viscoelastic Solids", *J. App. Mech.,* Vol. 59, pp. S43-S49. 1992.

7. Struik, C., Internal Stresses, Dimensional Instabilities, and Molecular orientations in Plastics, John Wiley and Sons, New York, NY. 1990.

8. Kawada, H. and Ikegami, K., "Viscoelastic Properties of Resin for IC Plastic Packages and Residual Stress", *JMSE Int. J.,* Series I, Vol. 35, No. 2, pp. 152-158. 1992.

9. Lee, E., et. al., "Residual Stresses in a Glass Plate Cooled Symmetrically from Both Surfaces", *J. Am. Ceramic Soc.,* Vol. 48, No. 9, pp. 480-487. 1965.

10. Lee, K. and Weitsman, Y., "Optimal Cool Down in Nonlinear Thermoviscoelasticity with Application to Graphite/PEEK (APC-2) Laminates", *J. App. Mech.,* Vol. 61, pp. 367-374. 1994.

11. Van Doorselaer, K. and DeZeeuw, K., "Relation between Delamination and Temperature Cycling Induced Failures in Plastic Packaged Devices", *IEEE Trans. on Comp., Hyb., and Man. Tech.,* Vol. 13, No. 4, pp. 879-882. 1990.

12. Chiou, B., et. al., "Temperature Cycling Effects between Sn/Pb Solder and Thick Film Pd/Ag conductor Metallization", *IEEE Trans. on Comp., Hyb., and Man. Tech.,* Vol. 14, No. 1, pp. 233-237. 1991.

13. McDonald, G. and Hendricks, R., "Effect of Thermal Cycling on Zr2O2-Y2O3 Thermal Barrier Coatings", *Thin Solid Films,* Vol. 73, pp. 491-496. 1980.

14. Kinloch, A. and Osiyemi, S., "Predicting the Fatigue Life of Adhesively-Bonded Joints", *J. Adh.,* Vol. 43, pp. 79-90. 1993.

15. Jiang, W., "The Elastic-Plastic Analysis of Tubes-IV: Thermal Ratchetting", *J. Pres. Ves. Tech., Trans. of ASME,* Vol. 114, No. 2, pp. 236-245. 1992.

16. Ryan, R. and Mall, S., "Cyclic Heating of a Layered Plate with an Interface Flaw", *J. Ther. Stresses,* Vol. 42, pp. 33-46. 1991.

17. Suresh, S., "Elastoplastic Analysis of Thermal Cycling: Layered Materials with Sharp Interfaces", *J. Mech. Phys. Solids,* Vol. 42, No. 6, pp. 979-1018. 1994.

18. Dunn, M. and Taya, M., "Creep and Thermal Cycling Creep of Metal Matrix Composites", *Thermomechanical Behavior of Advanced Structural Materials,* AD-Vol. 34/AMD-Vol. 173, pp. 33-46. ASME, 1993.

19. Lin, K. and Hwang, I., "Thermo-Viscoelastic Response of Graphite/Epoxy Composites", *J. Eng. Mat. Tech.,* Vol. 110, pp. 113-116. 1988.

20. Christensen, R., Theory of Viscoelasticity, 2nd ed., Academic Press, New York, NY. 1982.

21. Zienkiewicz, O., et. al., "A Numerical Method of Visco-elastic Stress Analysis", *Int. J. Mech. Sci.,* Vol. 10, pp. 807-827. 1968.

22. Williams, M., Landel, R., and Ferry J., "The Temperature Dependence of Relaxation Mechanisms in Amorphous Polymers and Other Glass-Forming Liquids", *J. Am. Chem. Soc.,* Vol. 77, pp. 3701-3706. 1955.

23. Shames, I., Mechanics of Deformable Solids, Robert Krieger Publishing, Malabar, FL. 1964

24. Chang, T., et. al., "Testing Methods for Accelerated Humidity Conditioning and Estimation of Adhesive Bond Durability", *J. Adh.,* Vol. 60, pp. 153. 1997.

25. Gorce, J., "Mechanical Hysterises of a Polyether Polyurethane Thermoplastic Elastomer", *Polymer Eng. and Sci.,* Vol. 33, No. 18, pp. 1170-1176. 1993.

26. Kinloch, A., "Adhesives in Engineering", Proc. Inst. Mech. Eng., Preprint, 84th Thomas Hawksley Memorial Lecture. Presented December 11, 1996.

27. Dillard, J., Professor of Chemistry, Virginia Tech. Personal communications, Summer 1996.

28. Rakestraw, M., et. al., "Time Dependent Crack Growth and Loading Rate Effects on Interfacial and Cohesive Fracture of Adhesive Joints", *J. Adh.,* Vol. 55, pp. 123-149. 1995.

29. Ward, T., Professor of Chemistry, Virginia Tech. Personal communications, Summer 1996.

Appendix A: Mathematica Routine

Mathematica routine for solution of recursive equation over 60 cycles given a near-square Tanh-wave thermal profile with a maximum and minimum of 70 and 27 degrees C respectively. Text documentation is delineated by bold print, input lines by normal text.

CONSTRAINED POLYMER BAR SUBJECTED TO THERMAL CYCLING

```
Needs["Graphics`Graphics`"]
```

Set material properties

```
k = 1*10^9;

tau=1;

c= k tau;

Tg = 87;

c1=20; c2=100;

alphao = .000100;

span=10; mult=2;

subst=0;
```

Set temperature cycling range

```
Tcold = 27;Thot = 70;
```

Select Time Step and Number of Cycles

```
dt=20;cyc=60;

upper=Round[cyc*3600/dt];
```

Temperature Profile

```
T[t_] = Tcold  +
  (Thot-Tcold)/2(Tanh[(t- 900)/120] - Tanh[(t- 2700)/120]);

Plot[T[t],{t,0,7200},PlotRange -> All,Frame->True]
```

Coefficient of Thermal Expansion

```
Ta=Tg-span/4;

Tb=Tg+span/4;

alp[T_]=alphao *
  (1 + (mult-1)/2 + (mult-1)/2 Tanh[3(T-(Ta+(Tb-Ta)/2))/(Tb-Ta)])-subst;

Plot[alp[t],{t,Tg-20,Tg+20},PlotRange -> {0,2.5 alphao}]
```

Define d(strain)/dt

```
dirstrain[t_] = alp[T[t]] D[T[t],t];
```

Temperature Profile

```
Ther = Table[0*j,{j,upper}];

Do[Ther[[i]]=N[T[i*dt]],{i,upper/cyc}]

If[cyc>1,
        Do[ Do[Ther[[i]]=Ther[[i-upper/cyc]],
          {i,j*upper/cyc+1,(j+1)*upper/cyc,1}],{j,1,cyc-1,1}]]
```

Shift Factor Array

```
a = Table[N[10^(c1 (Ther[[j]] - Tg)/(c2 + Ther[[j]] - Tg))],{j,upper}];
```

Calculate parameter arrays

```
po = 1;p1 = c/k;qo = 0;q1 = c;
```

Initialize variable arrays

```
curve=Table[0,{t,upper}];

edot=Table[0,{t,upper}];
```

Calculate forcing function arrays

```
Do[edot[[i]]=N[dirstrain[dt*i]],{i,upper/cyc}];

If[cyc>1,
  Do[ Do[edot[[i]]=edot[[i-upper/cyc]],
   {i,j*upper/cyc+1,(j+1)*upper/cyc,1}],{j,1,cyc-1,1}]];
```

Compute stresses

```
sigma=Table[0*t,{t,upper+1}];

fact=Table[-dt a[[i]]/tau,{i,upper}];

Do[

    If[fact[[i]]>-10^(-15),
      expon=N[1,250]+fact[[i]]+fact[[i]]^2,
      expon=E^fact[[i]]];

    sigma[[i+1]] = N[sigma[[i]] expon,250] + N[c/a[[i]] edot[[i]] (1-expon),250];

    curve[[i]] = {i*dt/3600,N[-sigma[[i+1]],250]},

{i,1,upper}];
```

Output plots

```
onecycle=Table[0,{t,2*upper/cyc}];

Do[onecycle[[i]] = {i*dt/3600,-sigma[[i+1]]/1000000},{i,1,2*upper/cyc}];

ListPlot[onecycle,
   PlotRange->All, AxesOrigin->{0,0},
        Frame->True, FrameLabel->{"Time (Hrs.)","Stress (MPa)"},
        PlotJoined->True,RotateLabel->False]

Do[curve[[i]] = {N[i*dt/3600],-sigma[[i+1]]/1000000},{i,1,upper}];

ListPlot[curve,
   PlotRange->All, AxesOrigin->{0,0},
        Frame->True, FrameLabel->{"Time (Hrs.)","Stress (MPa)"},
        PlotJoined->True,RotateLabel->False]

Max[-sigma]

Min[-sigma]
```

Appendix B: ABAQUS Input File - Stress Build-Up

ABAQUS Program for evaluation of stresses in one quarter of a symmetric sandwich-geometry adhesive bond subjected to near-square wave thermal loading between 27°C and 70°C. Only one cycle is included. Additional cycles are added by copying the four loading steps at the end and appending them to the file; each set of four loading steps is one cycle.

```
*HEADING
PUR layer on aluminum (2-D Analysis, Plane stress)
**
**Define nodes
*NODE,NSET=ALL
20,7.25,0.1
21,0.,1.2
22,8.,0.1
29,4.,1.2
30,10.,0.1
31,7.5,0.2
42,7.5,0.3
43,5.,1.2
45,6.,1.2
47,6.5,1.2
49,4.5,1.05
51,6.,1.05
53,7.5,0.4
64,7.25,0.5
65,5.,0.9
66,8.,0.5
71,6.5,0.9
73,5.,0.75
75,7.,0.6
76,7.5,0.6
77,8.,0.6
85,10.,0.6
87,6.,0.75
89,5.,0.6
95,6.5,0.6
98,7.5,0.9
109,0.,0.6
111,2,0.6
113,4.,0.6
115,4.5,0.3
117,6.,0.3
```

```
119,7.,1.2
120,7.5,1.2
121,8.,1.2
129,10.,1.2
130,7.,0.3
*NGEN,NSET=ALL
30,85,11
85,129,11
22,30,2
31,41,1
42,52,2
53,63,1
66,74,2
75,119,11
77,121,11
77,85,1
88,96,2
99,107,1
110,118,2
121,129,1
21,29,2
65,71,2
89,95,2
*NCOPY,CHANGE NUMBER=111,OLDSET=ALL,REFLECT=MIRROR,NEW SET=ALL
0.,0.,-1.
1.,0.,-1.
0.,0.,0.
*NODE,NSET=ALL
1,0.,0.
7,6.,0.
11,8.,0.
19,10.,0.
*NGEN,NSET=INTER
1,7,1
7,11,1
11,19,1
*NSET,NSET=ALL
INTER
**
**Define elements
*ELEMENT,TYPE=CPS8,ELSET=ADHES
1,1,3,25,21,2,111,23,109
2,3,5,29,25,4,113,27,111
3,5,89,65,29,115,73,49,113
4,5,7,93,89,6,117,91,115
5,7,9,75,93,8,130,95,117
6,89,93,69,65,91,87,67,73
```

```
7,93,75,97,69,95,86,71,87
8,65,69,45,29,67,51,43,49
9,69,97,119,45,71,108,47,51
10,9,31,53,75,20,42,64,130
11,9,11,33,31,10,22,32,20
*ELGEN,ELSET=ADHES
11,5,2,1,5,22,5
*ELEMENT,TYPE=CPS8,ELSET=METAL
36,3,1,132,136,2,220,134,222
37,5,3,136,140,4,222,138,224
38,5,140,176,200,224,160,184,226
39,7,5,200,204,6,226,202,228
40,9,7,204,186,8,228,206,241
41,204,200,176,180,202,184,178,198
42,186,204,180,208,206,198,182,197
43,180,176,140,156,178,160,154,162
44,208,180,156,230,182,162,158,219
45,9,186,164,142,241,175,153,131
46,11,9,142,144,10,131,143,133
51,144,142,164,166,143,153,165,155
*ELGEN,ELSET=METAL
46,5,2,1
51,5,2,1,4,22,5
**
**Define material properties
*MATERIAL,NAME=ALUM
*ELASTIC,TYPE=ISOTROPIC
73E3,0.3
*EXPANSION,ZERO=27.
0.000025
**
*MATERIAL,NAME=PUR
*ELASTIC,TYPE=ISOTROPIC
1000.,0.4
*VISCOELASTIC,TIME=PRONY
1.,0.0,1.
*TRS
87.,20.,100.
*EXPANSION,ZERO=27.
0.0001,27.
0.0001,82.
**
*SOLID SECTION,ELSET=SUBSTRATE,MATERIAL=ALUM
*SOLID SECTION,ELSET=ADHESIVE,MATERIAL=PUR
**
**Define Boundary Conditions
*BOUNDARY
```

```
LEFT,1,2
RIGHTSUB,2,2
**
**Define Thermal Cycling Parameters
*AMPLITUDE,NAME=UP,DEFINITION=TABULAR
0.,27.,400.,70.
*AMPLITUDE,NAME=HI,DEFINITION=TABULAR
0.,70.,1400.,70.
*AMPLITUDE,NAME=DOWN,DEFINITION=TABULAR
0.,70.,400.,27.
*AMPLITUDE,NAME=LO,DEFINITION=TABULAR
0.,27.,1400.,27.
**
**Apply Thermal Cycling
**Ramp Temperature Up
*STEP,INC=20
*VISCO,CETOL=5.E-1
20.,400.,20.,20.
*TEMPERATURE,AMPLITUDE=UP
ALL,1.
*EL PRINT,FREQ=10
S,TEMP
*NODE PRINT,FREQ=0
*RESTART,WRITE,FREQ=10
*END STEP
**
**Hold Hot Temperature
*STEP,INC=14
*VISCO,CETOL=5.E-1
100.,1400.,100.,100.
*TEMPERATURE,AMPLITUDE=HI
ALL,1.
*EL PRINT,FREQ=14
S,TEMP
*NODE PRINT,FREQ=0
*RESTART,WRITE,FREQ=14
*END STEP
**
**Ramp Temperature Down
*STEP,INC=20
*VISCO,CETOL=5.E-1
20.,400.,20.,20.
*TEMPERATURE,AMPLITUDE=DOWN
ALL,1.
*EL PRINT,FREQ=10
S,TEMP
*NODE PRINT,FREQ=0
```

```
*RESTART,WRITE,FREQ=10
*END STEP
**
**Hold Cold Temperature
*STEP,INC=14
*VISCO,CETOL=5.E-1
100.,1400.,100.,100.
*TEMPERATURE,AMPLITUDE=LO
ALL,1.
*EL PRINT,FREQ=14
S,TEMP
*NODE PRINT,FREQ=0
*RESTART,WRITE,FREQ=14
*END STEP
```

Appendix C: ABAQUS Input File - SERR Study

ABAQUS input file for evaluation of J-integral around a crack at the interface of a thermally-cycled layered (NCA) specimen for an applied tensile axial strain on the system. The input includes one thermal conditioning cycle. The input is modified from that originally created by Chang [24]. Additional cycles can be added by copying the four thermal loading steps at the end and appending them to the file before the J-integral calculation steps; each set of four loading steps is one thermal loading cycle.

```
*HEADING
NCA 2D WITH SINGULAR ELEMENTS
**
*************************************************************
**                  Modeling of NCA specimen
**
**Two dimensional analysis of NCA specimen
**Half of the specimen modeled
**Plane Stress Analysis
**Length = 40 mm
**Coating thickness = 0.15 mm
**Substrate thickness = 2 mm
**Crack at 5 mm from the tip
**Applied Thermal Profile - One Cycle
**Coating: Polyurethane, modulus = 1.0 GPa,
**Poisson's ratio = 0.4.
**Substrate: Aluminum, modulus = 73 GPa,
** Poisson's ratio = 0.3
**Displacement strains = .01, .03, .05, .07
**3 J-Integral contours around crack tip
*************************************************************
**
**Assign nodes at the corners
**
*NODE,NSET=ALL
**LEFT
1,0.,-2.
2,0.,-1.
3,0.,-0.15
4,0.,-0.1
5,0.,-0.065
6,0.,-0.055
7,0.,-0.045
```

```
8,0.,-0.035
9,0.,-0.025
10,0.,-0.01875
11,0.,-0.0125
12,0.,-0.00625
13,0.,0.
14,0.,0.00625
15,0.,0.0125
16,0.,0.01875
17,0.,0.025
18,0.,0.035
19,0.,0.045
20,0.,0.055
21,0.,0.065
22,0.,0.1
23,0.,0.15
**
**MID
438,34.96,-2.
439,34.96,-1.
440,34.96,-0.15
441,34.96,-0.1
442,34.96,-0.065
443,34.96,-0.055
444,34.96,-0.045
445,34.96,-0.035
446,34.96,-0.025
447,34.96,-0.01875
448,34.96,-0.0125
449,34.96,-0.00625
450,34.96,0.
451,34.96,0.00625
452,34.96,0.0125
453,34.96,0.01875
454,34.96,0.025
455,34.96,0.035
456,34.96,0.045
457,34.96,0.055
458,34.96,0.065
459,34.96,0.1
460,34.96,0.15
**
**MID1
461,34.975,-2.
462,34.975,-1.
463,34.975,-0.15
464,34.975,-0.1
```

```
465,34.975,-0.065
466,34.975,-0.055
467,34.975,-0.045
468,34.975,-0.035
469,34.975,-0.025
470,34.975,-0.01875
471,34.975,-0.0125
472,34.975,-0.00625
473,34.975,0.
474,34.975,0.
475,34.975,0.00625
476,34.975,0.0125
477,34.975,0.01875
478,34.975,0.025
479,34.975,0.035
480,34.975,0.045
481,34.975,0.055
482,34.975,0.065
483,34.975,0.1
484,34.975,0.15
**
**MID2
653,35.025,-2.
654,35.025,-1.
655,35.025,-0.15
656,35.025,-0.1
657,35.025,-0.065
658,35.025,-0.055
659,35.025,-0.045
660,35.025,-0.035
661,35.025,-0.025
662,35.025,-0.01875
663,35.025,-0.0125
664,35.025,-0.00625
665,35.025,0.
666,35.025,0.
667,35.025,0.00625
668,35.025,0.0125
669,35.025,0.01875
670,35.025,0.025
671,35.025,0.035
672,35.025,0.045
673,35.025,0.055
674,35.025,0.065
675,35.025,0.1
676,35.025,0.15
**
```

```
**RIGHT
893,40.,-2.
894,40.,-1.
895,40.,-0.15
896,40.,-0.1
897,40.,-0.065
898,40.,-0.055
899,40.,-0.045
900,40.,-0.035
901,40.,-0.025
902,40.,-0.01875
903,40.,-0.0125
904,40.,-0.00625
905,40.,0.
906,40.,0.
907,40.,0.00625
908,40.,0.0125
909,40.,0.01875
910,40.,0.025
911,40.,0.035
912,40.,0.045
913,40.,0.055
914,40.,0.065
915,40.,0.1
916,40.,0.15
**
**Nodes around singular elements
1000,35.,0.
1224,35.,0.
1006,35.025,0.
1034,35.025,0.025
1090,34.975,0.025
1146,34.975,-0.025
1202,35.025,-0.025
1230,35.025,0.
**
**Generate node sets
*NSET,NSET=LEFT,GENERATE
1,23
*NSET,NSET=MID,GENERATE
438,460
*NSET,NSET=MID1,GENERATE
461,484
*NSET,NSET=MID2,GENERATE
653,676
*NSET,NSET=RIGHTSUB,GENERATE
893,905
```

```
*NSET,NSET=RIGHTADH,GENERATE
906,916
*NSET,NSET=RIGHT,GENERATE
893,916
*NGEN,NSET=TIP
1000,1224,7
*NGEN,NSET=OUTER
1006,1034,7
1034,1090,7
1090,1146,7
1146,1202,7
1202,1230,7
*NFIL,BIAS=1.5
LEFT,MID,19,23
*NFIL,BIAS=0.5
MID2,RIGHT,10,24
*NFIL
MID1,MID2,8,24
*NFIL,SINGULAR=1
TIP,OUTER,6,1
*NSET,NSET=ALL,GENERATE
1,1230
**
**Define elements
*ELEMENT,TYPE=CPS8R
**Define left corner elements
1,1,47,49,3,24,48,26,2
111,461,509,511,463,485,510,487,462
127,480,528,530,482,504,529,506,481
139,701,749,751,703,725,750,727,702
201,13,59,61,15,36,60,38,14
401,714,762,764,716,738,763,740,715
**
**Define elements around singular elements
531,421,467,1146,423,444,468,446,422
532,467,515,1160,1146,491,516,1153,468
533,515,563,1174,1160,539,564,1167,516
534,563,611,1188,1174,587,612,1181,564
535,611,659,1202,1188,635,660,1195,612
536,659,707,709,1202,683,708,685,660
537,1202,709,711,1216,685,710,687,1209
538,1216,711,713,1230,687,712,689,1223
539,423,1146,1132,425,446,1139,448,424
540,425,1132,1118,427,448,1125,450,426
541,427,1118,1104,429,450,1111,452,428
542,429,1104,1090,431,452,1097,454,430
543,1006,714,716,1020,690,715,692,1013
```

```
544,1020,716,718,1034,692,717,694,1027
545,431,1090,480,433,454,479,456,432
546,1090,1076,528,480,1083,527,504,479
547,1076,1062,576,528,1069,575,552,527
548,1062,1048,624,576,1055,623,600,575
549,1048,1034,672,624,1041,671,648,623
550,1034,718,720,672,694,719,696,671
**
**Define elements under singular elements
801,415,461,463,417,438,462,440,416
802,417,463,465,419,440,464,442,418
803,419,465,467,421,442,466,444,420
804,653,701,703,655,677,702,679,654
805,655,703,705,657,679,704,681,656
806,657,705,707,659,681,706,683,658
**
**Define elements above singular elements
807,433,480,482,435,456,481,458,434
808,435,482,484,437,458,483,460,436
809,672,720,722,674,696,721,698,673
810,674,722,724,676,698,723,700,675
**
**Define first singular element
300,1000,1002,1016,1014,1001,1009,1015,1007
**
**Generate elements in substrate
*ELGEN
300,3,2,1,16,14,3
*ELGEN,ELSET=SUBSTRATE
1,9,46,1,6,2,9
111,4,48,1,3,2,4
139,4,48,1,6,2,4
*ELSET,ELSET=SUBSTRATE,GENERATE
801,806
531,540
324,347
**
**Generate elements in coating
*ELGEN,ELSET=ADHESIVE
201,9,46,1,5,2,9
127,4,48,1,2,2,4
401,4,48,1,5,2,4
*ELSET,ELSET=ADHESIVE,GENERATE
541,550
807,810
300,323
**
```

```
**Define material properties
*MATERIAL,NAME=ALUM
*ELASTIC,TYPE=ISOTROPIC
73E3,0.3
*EXPANSION,ZERO=27.
0.000025
**
*MATERIAL,NAME=PUR
*ELASTIC,TYPE=ISOTROPIC
1000.,0.4
*VISCOELASTIC,TIME=PRONY
1.,0.0,1.
*TRS
87.,20.,100.
*EXPANSION,ZERO=27.
0.0001,27.
0.0001,82.
**
*SOLID SECTION,ELSET=SUBSTRATE,MATERIAL=ALUM
*SOLID SECTION,ELSET=ADHESIVE,MATERIAL=PUR
**
**Define Boundary Conditions
*BOUNDARY
LEFT,1,2
RIGHTSUB,2,2
**
**Define Thermal Cycling Parameters
*AMPLITUDE,NAME=UP,DEFINITION=TABULAR
0.,27.,400.,70.
*AMPLITUDE,NAME=HI,DEFINITION=TABULAR
0.,70.,1400.,70.
*AMPLITUDE,NAME=DOWN,DEFINITION=TABULAR
0.,70.,400.,27.
*AMPLITUDE,NAME=LO,DEFINITION=TABULAR
0.,27.,1400.,27.
**
**Apply Thermal Cycling
**Ramp Temperature Up
*STEP,INC=400
*VISCO,CETOL=5.E-1
1.,400.,1.,1.
*TEMPERATURE,AMPLITUDE=UP
ALL,1.
*EL PRINT,FREQ=400
S,TEMP
*NODE PRINT,FREQ=0
*RESTART,WRITE,FREQ=0
```

```
*END STEP
**
**Hold Hot Temperature
*STEP,INC=14
*VISCO,CETOL=5.E-1
100.,1400.,100.,100.
*TEMPERATURE,AMPLITUDE=HI
ALL,1.
*EL PRINT,FREQ=14
S,TEMP
*NODE PRINT,FREQ=0
*RESTART,WRITE,FREQ=14
*END STEP
**
**Ramp Temperature Down
*STEP,INC=400
*VISCO,CETOL=5.E-1
1.,400.,1.,1.
*TEMPERATURE,AMPLITUDE=DOWN
ALL,1.
*EL PRINT,FREQ=400
S,TEMP
*NODE PRINT,FREQ=0
*RESTART,WRITE,FREQ=0
*END STEP
**
**Hold Cold Temperature
*STEP,INC=14
*VISCO,CETOL=5.E-1
100.,1400.,100.,100.
*TEMPERATURE,AMPLITUDE=LO
ALL,1.
*EL PRINT,FREQ=14
S,TEMP
*NODE PRINT,FREQ=0
*RESTART,WRITE,FREQ=14
*END STEP
**
**Do J-Integral for each of four applied strains
**1% Strain
*STEP
*STATIC
*BOUNDARY
RIGHTSUB,1,1,0.4
*J-INTEGRAL,CONTOURS=3
0.0,1.0
TIP
```

```
*NODE PRINT
U
*RESTART,WRITE
*END STEP
**
**3% Strain
*STEP
*STATIC
*BOUNDARY
RIGHTSUB,1,1,1.2
*J-INTEGRAL,CONTOURS=3
0.0,1.0
TIP
*NODE PRINT
U
*RESTART,WRITE
*END STEP
**
**5% Strain
*STEP
*STATIC
*BOUNDARY
RIGHTSUB,1,1,2.0
*J-INTEGRAL,CONTOURS=3
0.0,1.0
TIP
*NODE PRINT
U
*RESTART,WRITE
*END STEP
**
**7% Strain
*STEP
*STATIC
*BOUNDARY
RIGHTSUB,1,1,2.8
*J-INTEGRAL,CONTOURS=3
0.0,1.0
TIP
*NODE PRINT
U
*RESTART,WRITE
*END STEP
```

Appendix D: Experimental Results

Page 64: DMA Data, first heating cycle
Page 65: DMA Data, second heating cycle
Page 66: DSC Data, first and scond heating cycles
Page 67: DDSC Data, first heating cycle
Page 68: DDSC Data, second heating cycle
Page 69: Plot of typical DCB loading curve data
Page 70: Linear data fit for DCB compliance method analysis
Page 71: DCB data from testing polyurethane-aluminum system
Page 72: SERR vs. time data for a sub-ambient DCB test

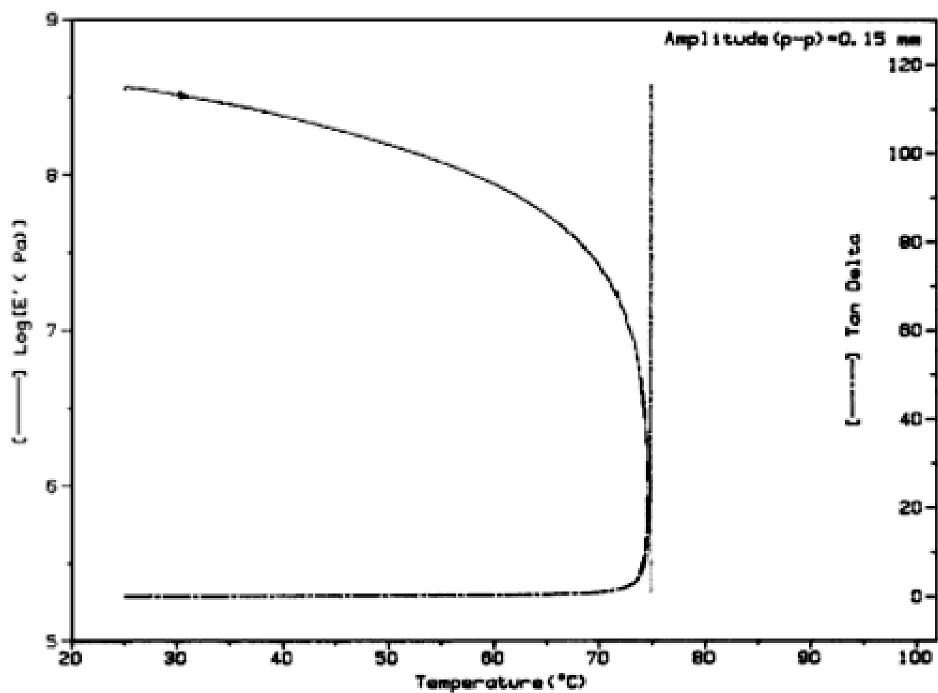

Figure 32. DMA Data, First Heating Cycles

Modulus gradually decreases over the first part of the heating cycle, dropping off more quickly and eventually becoming entirely rubbery around 75°C.

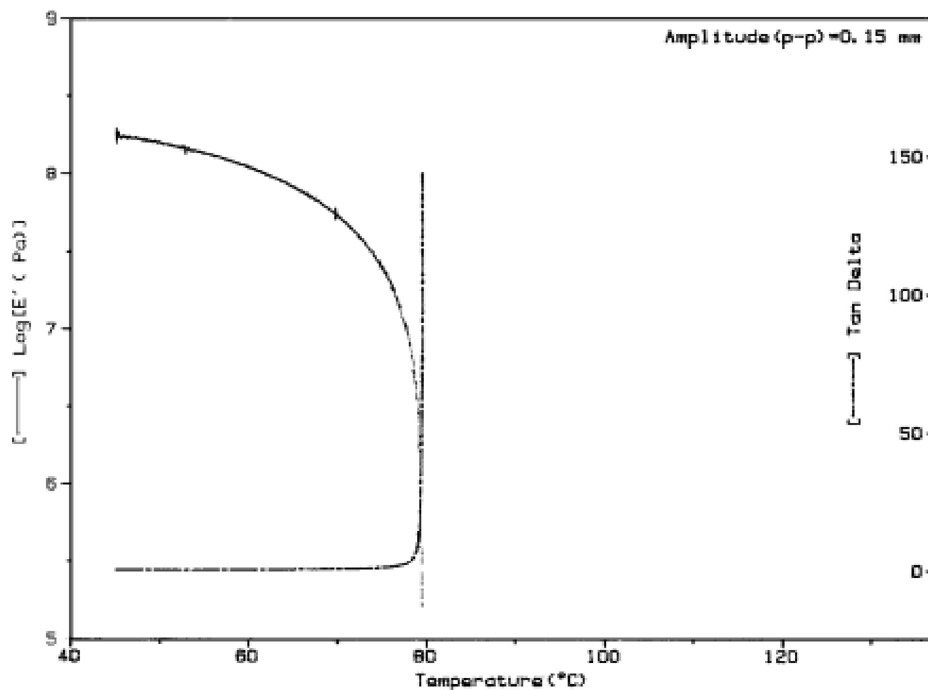

Figure 33. DMA Data, Second Heating Cycles

Modulus again drops off as it is heated, but temperature at which it no longer can sustain mechanical load has shifted to 80°C. Note that the scale on the x-axis is not the same as the previous plot.

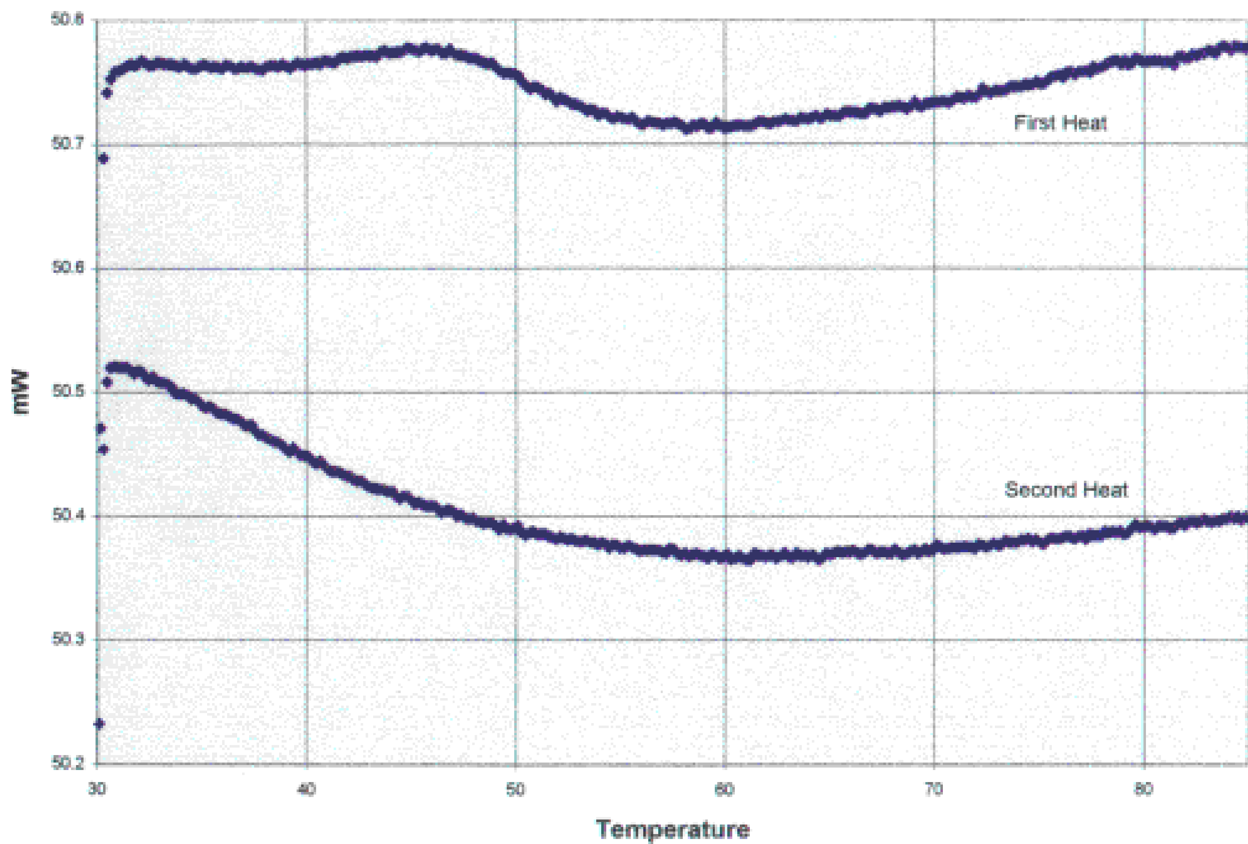

Figure 34. DSC Data, First and Second Heating Cycles

A transition seems evident around 50°C on the first cycle, but is not revealed in the data from the second heating cycle.

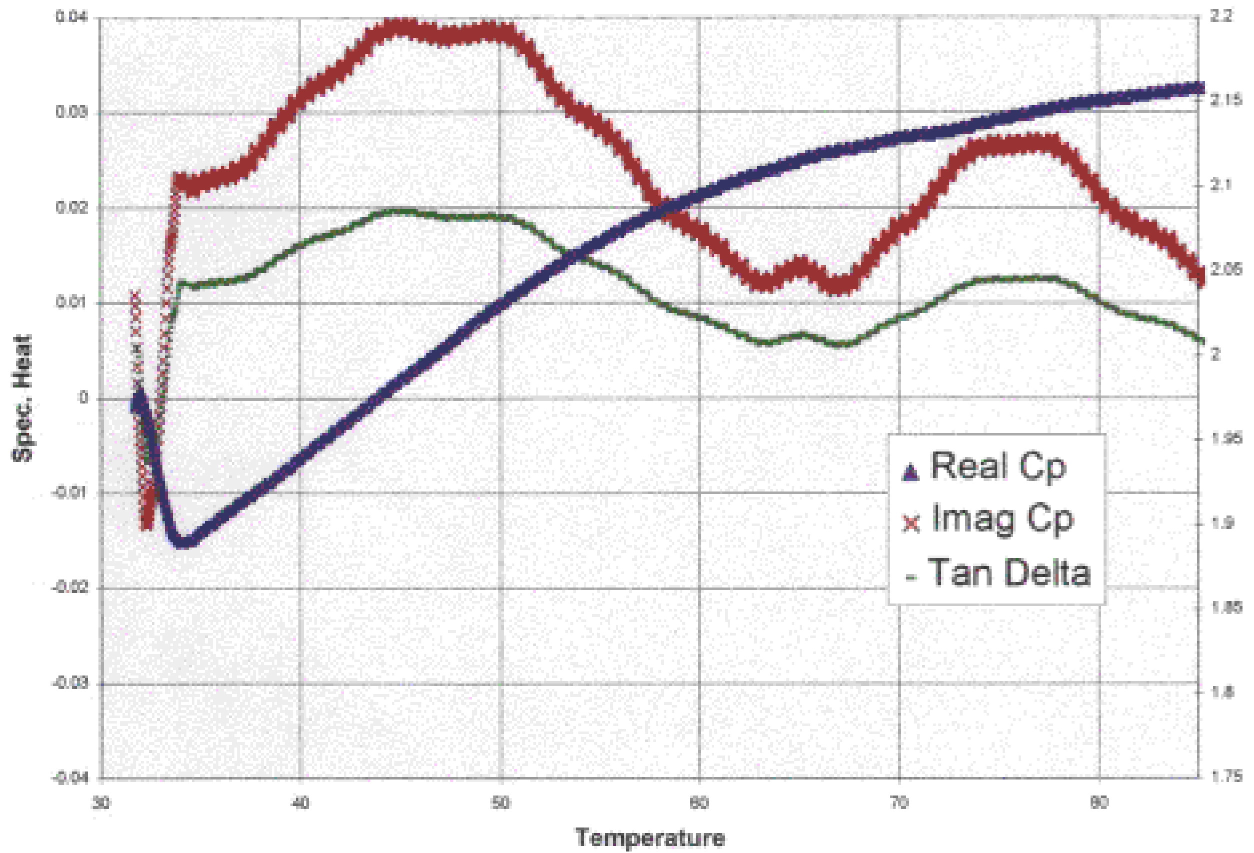

Figure 35. DDSC Data, First Heating Cycle

Note the hump in Imaginary Cp curve around 50°C. The second hump may represent another transition, corresponding with the drop in stiffness shown by the DMA data

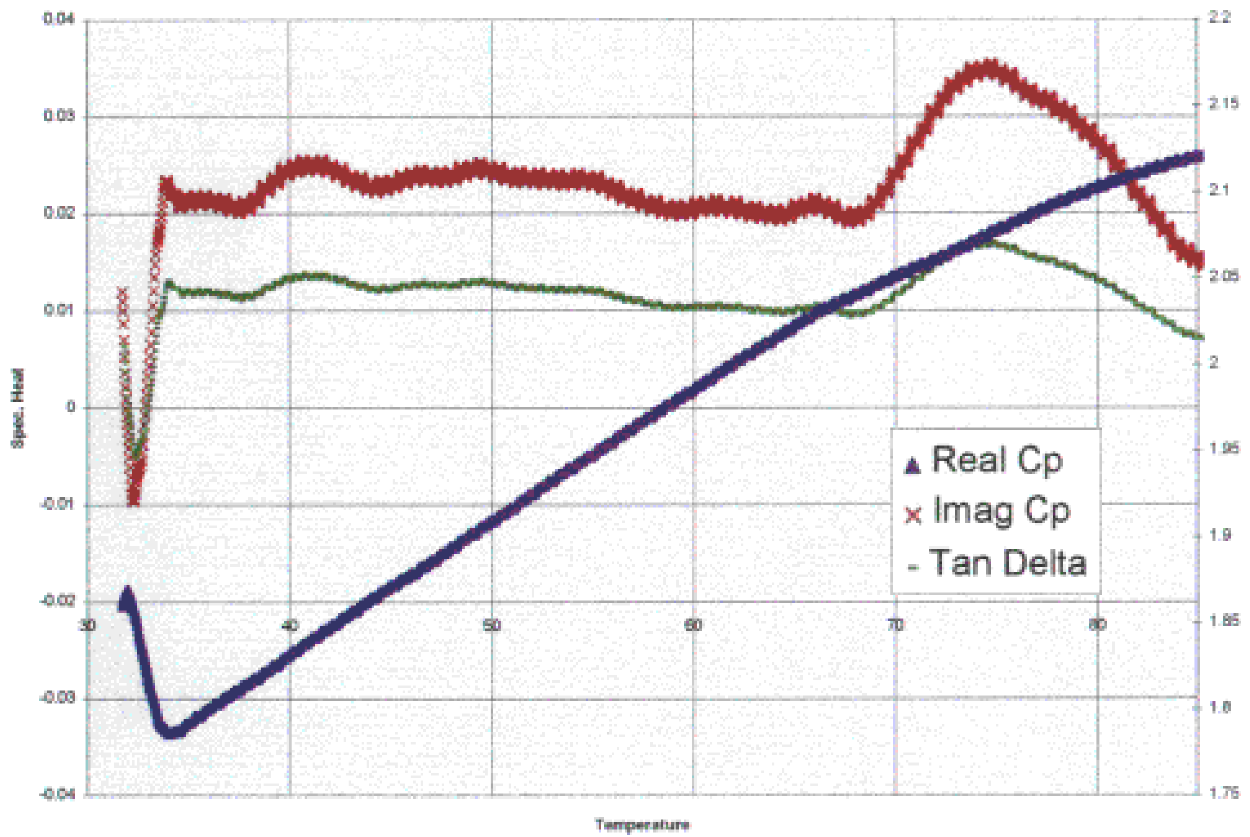

Figure 36. DDSC Data, Second Heating Cycle

The hump in Imaginary Cp curve around 50°C has disappeared. This is evidence of some irreversible chemical changes occuring in the sample during the first heating cycle. The second hump remains; perhaps it represents the glass transition.

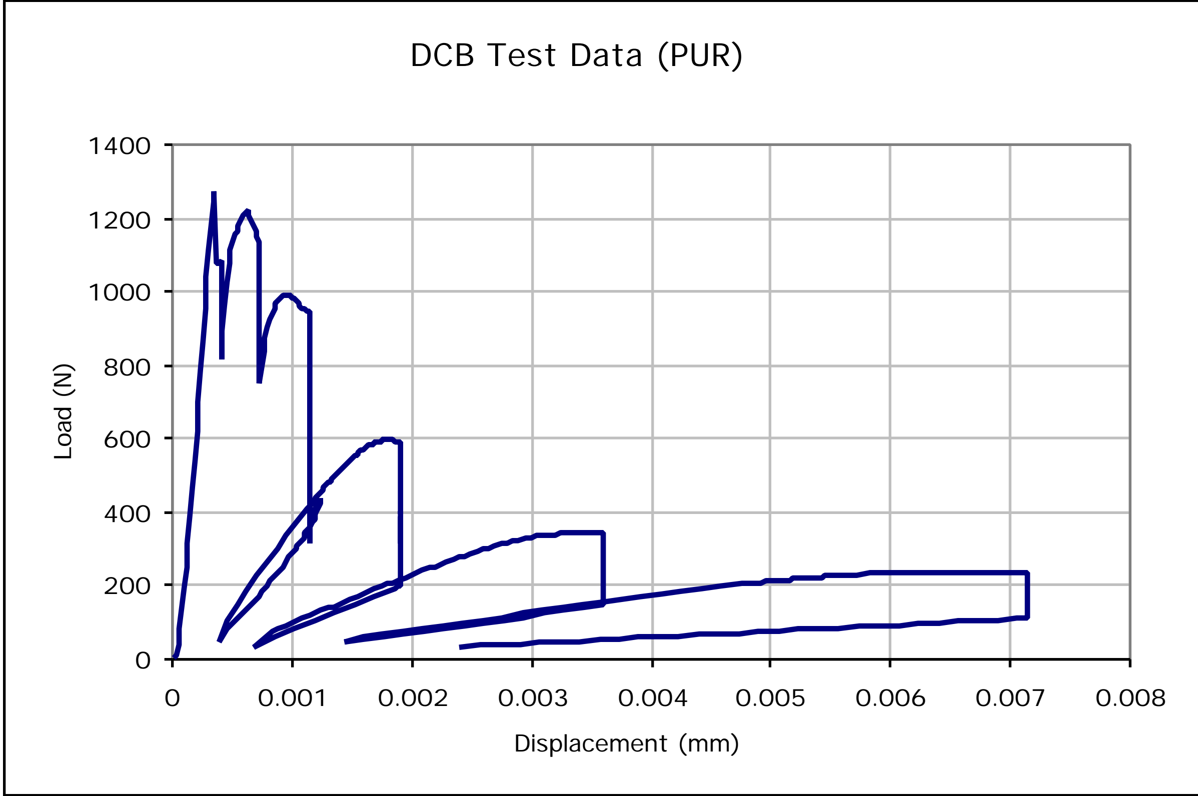

Figure 37. Plot of typical quasi-static DCB loading curve

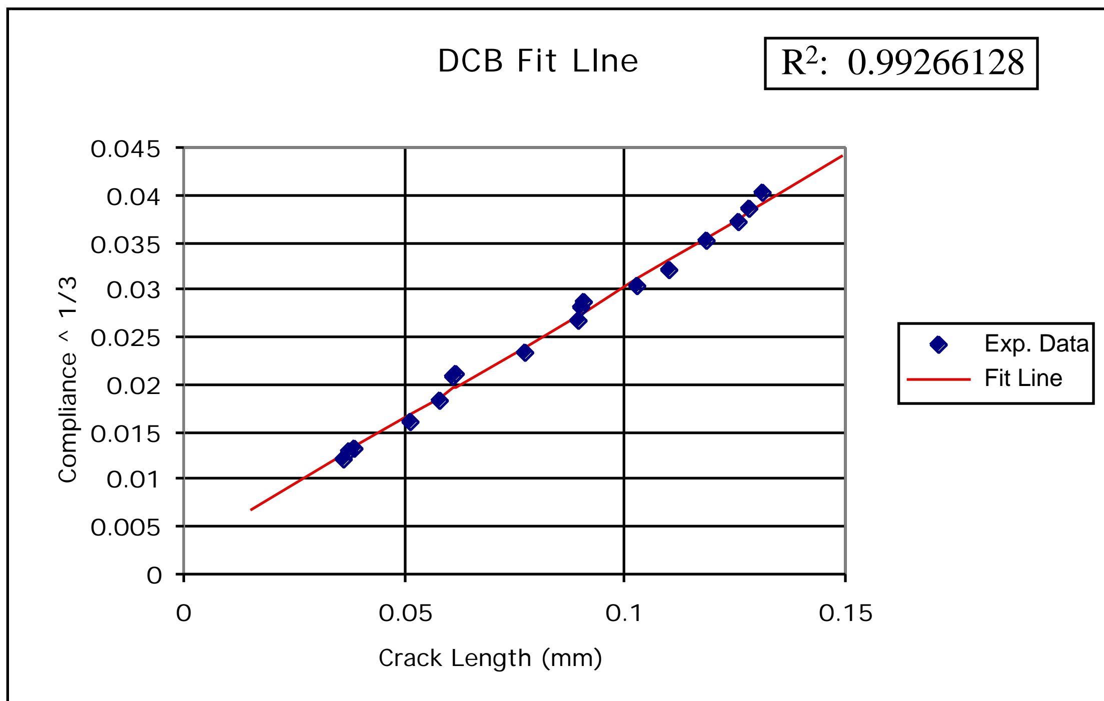

Figure 38. Data fit for typical compliance method DCB analysis

Specimen	G_c (J/m^2)	Std. Dev.	Points
Grit Blast Only	211.48	20.11	4
	212.93	13.55	3
Etch Only	90.79	12.82	3
Grit & Etch	121.30	3.38	2
	80.41	11.35	3
	51.06	4.68	7
(Cold Tests)	541.40	496.43	4
	804.16	434.19	7

Figure 39. Data acquired from quasi-static DCB testing of Al-PUR bonds

Specimens with different surface pre-treatements were tested. The specimens with grit-blasted surfaces had the most consisent data, and the recommended surface pre-treatment (Grit & Etch) resulted in much lower values and less consistent values. Testing at sub-ambient temperatures raised the fracture toughness on average, but error was very large for those tests due to changing temperature in the load cell affecting the readings.

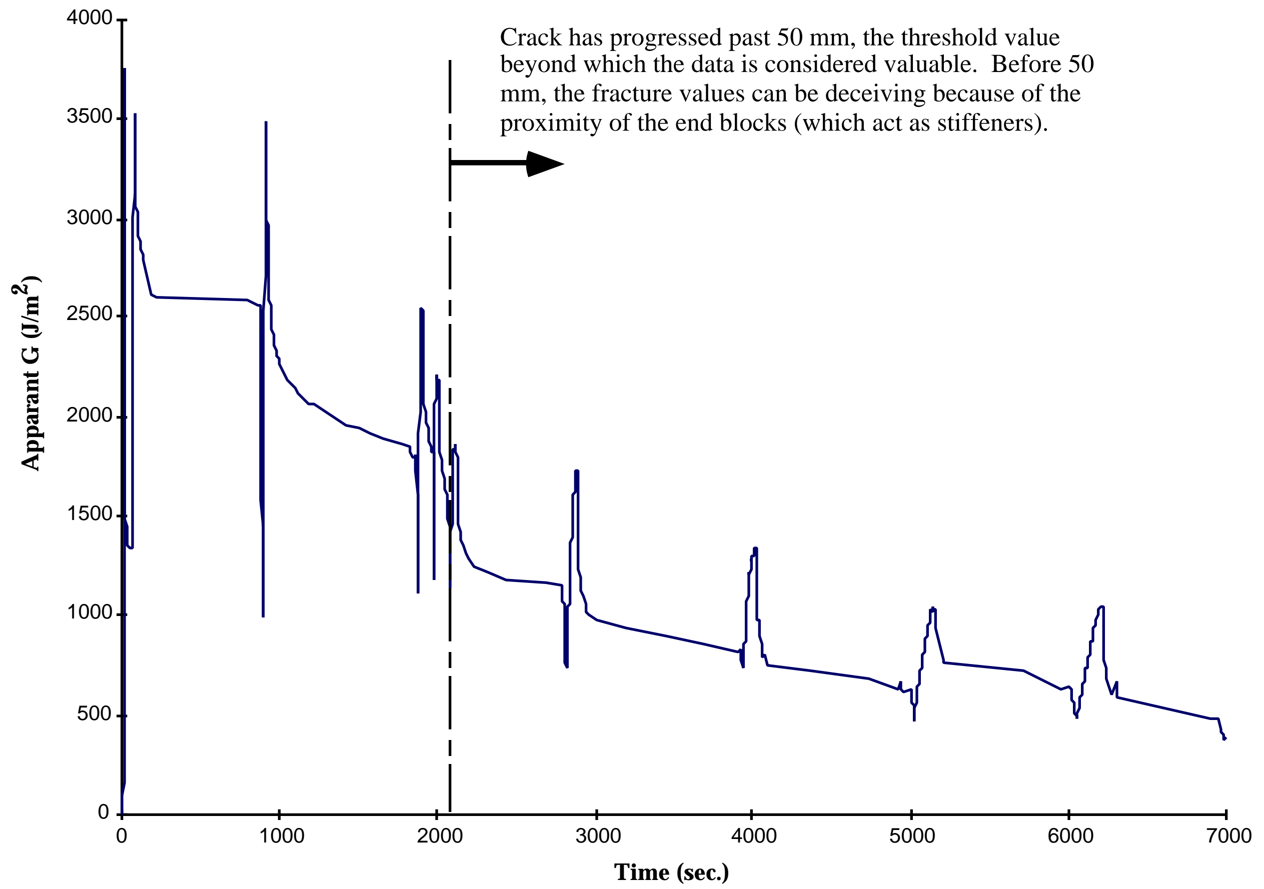

Figure 40. Plot of G vs. Time for sub-ambient DCB test.

G should level off for each cycle rather than decrease.

Vita

George Robert “Rob” Humfeld, Jr. was born to George and Diana Humfeld on November 16, 1970 in Fairfax, Virginia. Almost all of his childhood was spent in Reston, Virginia, where he pursued soccer, French horn, German language, and travel as his activities of greatest interest. His five years of undergraduate studies (1988-1993) in Engineering Mechanics at Virginia Tech included one year of study abroad in Braunschweig, Germany and many hours of canoeing and fishing on the New River. The author’s entry into the Engineering Mechanics graduate program at Virginia Tech in 1994 was preceded by a year working at the National Laboratory in Oak Ridge, Tennessee. While in graduate school, he found time to begin his own home business in telecommunications which he hopes to build part-time in the coming years. The first step of the career path of the author after graduation has yet to reveal itself, but will most likely lead to an industry engineering job in the foreseeable future.